Li et al. *Zool. Res.* 2022, 43(4): 497−513
https://doi.org/10.24272/j.issn.2095-8137.2022.011

ZR | Zoological Research

Article Open Access

Fuel source shift or cost reduction: Context-dependent adaptation strategies in closely related *Neodon fuscus* and *Lasiopodomys brandtii* against hypoxia

Xiu-Juan Li[1,#], Cong-Cong Qiao[1,#], Bo-Jian Chen[2,3,#], Meng-Yang Li[1], Peng Chen[4,5], Mao-Lin Huang[1], Chun-Xiao Chen[1], Yan Liu[1], Han Cheng[1], Meng-Wan Jiang[6], Lu-Ye Shi[1,4,*], Zhen-Long Wang[1,*]

[1] *School of Life Sciences*, *Zhengzhou University*, *Zhengzhou*, *Henan* 450001, *China*

[2] *College of Environmental Science and Engineering*, *Tongji University*, *Shanghai* 200092, *China*

[3] *Jiaxing-Tongji Environmental Research Institute*, *Jiaxing*, *Zhejiang* 314051, *China*

[4] *State Key Laboratory of Genetic Resources and Evolution*, *Kunming Institute of Zoology*, *Chinese Academy of Sciences*, *Kunming*, *Yunnan* 650223, *China*

[5] *Kunming College of Life Science*, *University of Chinese Academy of Sciences*, *Kunming*, *Yunnan* 650223, *China*

[6] *School of Artificial Intelligence and Big Data*, *Henan University of Technology*, *Zhengzhou*, *Henan* 450001, *China*

ABSTRACT

Oxygen is essential for most life forms. Insufficient oxygen supply can disrupt homeostasis and compromise survival, and hypoxia-induced cardiovascular failure is fatal in many animals, including humans. However, certain species have adapted and evolved to cope with hypoxic environments and are therefore good models for studying the regulatory mechanisms underlying responses to hypoxia. Here, we explored the physiological and molecular responses of the cardiovascular system in two closely related hypoxia-adapted species with different life histories, namely, Qinghai voles (*Neodon fuscus*) and Brandt's voles (*Lasiopodomys brandtii*), under hypoxic (10% O_2 for 48 h) and normoxic (20.9% O_2 for 48 h) exposure. Kunming mice (*Mus musculus*) were used for comparison. Qinghai voles live in plateau areas under hypoxic conditions, whereas Brandt's voles only experience periodic hypoxia. Histological and hematological analyses indicated a strong tolerance to hypoxia in both species, but significant cardiac tissue damage and increased blood circulation resistance in mice exposed to hypoxia. Comparative transcriptome analysis revealed enhanced oxygen transport efficiency as a coping mechanism against hypoxia in both *N. fuscus* and *L. brandtii*, but with some differences. Specifically, *N. fuscus* showed up-regulated expression of genes related to accelerated cardiac contraction and angiogenesis, whereas *L. brandtii* showed significant up-regulation of erythropoiesis-related genes. Synchronized up-regulation of hemoglobin synthesis-related genes was observed in both species. In addition, differences in cardiometabolic strategies against hypoxia were observed in the rodents. Notably, *M.*

Received: 07 March 2022; Accepted: 05 May 2022; Online: 11 May 2022

Foundation items: This work was supported by the National Natural Science Foundation of China (U2004152), Zhongyuan Science and Technology Innovation Leading Talent Project (224200510001), and China Postdoctoral Science Foundation (2020M672264)

[#]Authors contributed equally to this work

*Corresponding authors, E-mail: sly@zzu.edu.cn; wzl@zzu.edu.cn

musculus relied on adenosine triphosphate (ATP) generation via fatty acid oxidation, whereas *N. fuscus* shifted energy production to glucose oxidation under hypoxic conditions and *L. brandtii* employed a conservative strategy involving down-regulation of fatty acid and glucose oxidation and a bradycardia phenotype. In conclusion, the cardiovascular systems of *N. fuscus* and *L. brandtii* have evolved different adaptation strategies to enhance oxygen transport capacity and conserve energy under hypoxia. Our findings suggest that the coping mechanisms underlying hypoxia tolerance in these closely related species are context dependent.

Keywords: Heart; Hypoxia; *Lasiopodomys brandtii*; *Neodon fuscus*; RNA sequencing

INTRODUCTION

Oxygen is essential for the survival of most life forms and plays an important role in cellular aerobic energy supply and whole-body homeostasis (López-Barneo et al., 2001; Majmundar et al., 2010; Thompson, 2016). A decrease in ambient oxygen can impair various physiological processes and trigger pathological reactions, thereby limiting organism survival in hypoxic environments, such as found at high altitude (Shao et al., 2021; Suzuki et al., 2019). Tissue-level hypoxia is often fatal and epidemiological studies have revealed that hypoxia is a principal cause of cardiovascular and cerebrovascular diseases, which are common causes of human death in industrialized societies (Chen et al., 2019; Iacobas et al., 2008). Hypoxia can also stimulate the production of reactive oxygen species in tissues, leading to oxidative stress and even death in severe cases (Hermes-Lima & Zenteno-Savín, 2002; Lau et al., 2019). Therefore, understanding the response mechanisms to hypoxia is of great significance for the protection of humans and other animals in hypoxic environments and for diagnosis of hypoxia-related diseases (Zhang et al., 2020).

The heart is a highly oxygen-consumptive organ and provides oxygen and nutrients to the body by continuously boosting blood flow (Katano et al., 2019). Therefore, a sustainable and sufficient oxygen supply is essential for normal cardiac function (Huang et al., 2021; Pell et al., 2016). Hypoxia can cause heart rate alteration, cardiac output disorder, blood pressure elevation, myocardial dysfunction, irreversible myocardial cell apoptosis, and even death (Khodaee et al., 2016; Paparde et al., 2015). However, some animals that live in hypoxic environments have evolved morphological and physiological cardiovascular adaptations to cope with such conditions, such as larger hearts, higher mitochondrial surface density, and greater microvascular density (Pichon et al., 2013; Wang et al., 2021). In terms of cardiac metabolism, some species have evolved improved energy efficiency by enhancing carbohydrate metabolism (Duan et al., 2021; Schippers et al., 2012; Su et al., 2021). Thus, these animals are considered good models for studying the regulatory mechanisms involved in the cardiovascular system in response to hypoxia.

The Qinghai vole (*Neodon fuscus*) is an endemic species distributed in the alpine meadows, swamp grasslands, and shrub grasslands of the Qinghai-Xizang (Tibet) Plateau, at elevations of 3 700–4 800 m a.s.l. (Zhang et al., 2013, 2018). This small rodent has evolved a unique set of adaptation strategies to cope with its hypoxic environment, including more efficient oxygen transport capacity and lower risk of thrombosis (Li et al., 2021b). Brandt's vole (*Lasiopodomys brandtii*) is closely related to *N. fuscus* (with both previously belonging to the genus *Lasiopodomys*) and is mainly distributed in the temperate grasslands of Inner Mongolia, southeastern Mongolia, and parts of southern Russia, at an average elevation of <1 000 m a.s.l. (Liu et al., 2020; Shi et al., 2021a). Qinghai voles live in a persistently hypoxic environment, whereas Brandt's voles only experience relatively mild and periodic hypoxia when gathered underground during specific periods, such as at rest. However, empirical studies suggest that *L. brandtii* also exhibits extraordinary tolerance to hypoxia (Dong et al., 2018; Li et al., 2021c; Shi et al., 2021b, 2021c). Although these two species are closely related, their different habitats and life history patterns may have contributed to differences in hypoxic adaptations. Therefore, in the present study, we examined whether the high hypoxia tolerance of these two closely related species is achieved through different coping mechanisms and strategies. We conducted comparative physiological and transcriptomics analyses to investigate changes in cardiac tissue structure, blood parameters, and mRNA expression in *N. fuscus*, *L. brandtii*, and Kunming mice (*Mus musculus*) under hypoxic (10% O_2 for 48 h) and normoxic (20.9% O_2 for 48 h) conditions.

MATERIALS AND METHODS

Ethics statement

All protocols used in the present study were approved by the Institutional Animal Care and Use Committee, Zhengzhou University, Zhengzhou, Henan, China (permit No. ZZUIRB2022-44), and were carried out in accordance with the approved guidelines for the Use of Experimental Animals (China). All local regulations and laws were strictly followed.

Animals and acclimation

The *N. fuscus* voles were captured in the Guoluo Tibetan Autonomous Prefecture, Qinghai Province, China (N34°8′, E100°11′). The *L. brandtii* voles were purchased from the Chinese Academy of Agricultural Sciences (Beijing, China). The Kunming mice was purchased from the Laboratory Animal Center of Henan Province (Zhengzhou, China). All experimental animals were raised individually in uniformly sized polycarbonate boxes (length×width×height, 290 mm×178 mm×160 mm). Air temperature was 20–24 °C, relative humidity was 35%–50%, and photoperiod was 12 h light:12 h dark. Animals were fed mixed commercial rat feed and rabbit feed (Henan Experimental Animal Center, Zhengzhou, Henan Province, China) as well as fresh carrots and water *ad libitum*. All experimental animals were domesticated in the laboratory for at least eight weeks.

Hypoxia treatment

After acclimation, 18 adult females of similar size were selected from each species and randomly divided into two groups: hypoxia treatment group (10% O_2 for 48 h, *n*=9) and normoxia treatment group (20.9% O_2 for 48 h, *n*=9). Hypoxic treatment was conducted in December using hypoxic chambers (DS-II hyperbaric cabin, Huaxin Hyperbaric Cabin, China), with the O_2 level monitored in real time using an oxygen analyzer. A bottle containing sodium hydroxide was placed in the cabin to absorb the carbon dioxide released by the animals. Animals in the normoxia treatment group were also placed in a sealed oxygen chamber for 48 h. Except for the oxygen content, all other environmental conditions were constant for all groups. No mortality occurred during hypoxia/normoxia treatment. After hypoxia/normoxia treatment, all experimental animals were euthanized immediately by an intraperitoneal overdose injection of pentobarbital sodium (30 mg/kg) and whole hearts were removed for further analysis. Histological and hematological analyses were performed in six of the nine animals of each species in each group and transcriptome sequencing after RNA extraction was conducted in the remaining three animals from each group.

Histological evaluation

Whole hearts were collected from the animals and fixed in 4% paraformaldehyde for more than 24 h, dehydrated with ethanol, embedded in paraffin, and sectioned into 4 μm thick sections, which were processed and stained with hematoxylin and eosin (H&E) and Masson trichrome to evaluate tissue damage. H&E-stained sections of the cardiac apex of normoxic and hypoxic groups were examined under a light microscope (BX53 fluorescence microscope, Olympus Corporation, Japan) at 200× magnification. Masson staining was performed to assess the degree of cardiac fibrosis in five randomly selected visual fields (400× magnification) in each sample by calculating the percentage of blue-stained area (corresponding to fibrosis) relative to total heart area using ImageJ v1.53 (Wang et al., 2018). GraphPad Prism v8.0.1 (GraphPad Software, USA) was used to analyze and graph differences in cardiac fibrosis among the six samples from the normoxic and hypoxic treatment groups with independent sample *t*-test. Data are presented as mean±standard error of the mean (*SEM*) and $P<0.05$ was considered statistically significant.

Measurement of hematological parameters

Fresh blood samples from the three species were collected in ethylenediamine tetra-acetic acid (EDTA)-anticoagulated tubes to measure erythrocyte system parameters using an automated hematology analyzer (BC-2800Vet, Mindray, China), including red blood cells (RBC), hemoglobin (HGB), hematocrit (HCT), mean corpuscular volume (MCV), mean red blood cell hemoglobin (MCH), mean red blood cell hemoglobin concentration (MCHC), and red blood cell distribution width (RDW). GraphPad Prism v8.0.1 was used to analyze and graph the differences between the normoxic and hypoxic treatment groups using independent sample *t*-test. Data are presented as mean±*SEM* and $P<0.05$ was considered statistically significant.

RNA extraction, cDNA library construction, and RNA sequencing (RNA-seq)

Total RNA was extracted from heart tissue using TRIzol reagent (Invitrogen, USA) according to the manufacturer's instructions. RNA quality was assessed by: (1) analysis of RNA integrity by agarose gel electrophoresis (1.0%); (2) measurement of RNA concentration and purity using a NanoDropND-1000 spectrophotometer (NanoDrop Technologies, LLC, USA); and (3) accurate detection of RNA integrity number (RIN) using an Agilent 2100 bioanalyzer (Agilent Technologies, USA). RNA samples meeting these standards were added with oligo (dT) magnetic beads to enrich mRNA with poly-A tails, which were then broken into short fragments (250–300 bp) using fragmentation buffer and used as a template to synthesize first- and second-strand cDNA. The obtained double-stranded cDNA was then purified using AMPure XP beads and subjected to end-repair, poly-A tail addition, sequencing adaptor ligation, fragment size selection, and polymerase chain reaction (PCR) amplification for cDNA library construction. Finally, the Illumina NovaSeq 6000 platform was used to perform next-generation paired-end sequencing of the constructed cDNA library, with 150 paired-end reads and >6 Gb of raw data per sample. The remaining RNA samples were reverse-transcribed into cDNA using a PrimeScript RT Reagent Kit and gDNA Eraser (TaKaRa, Japan) according to the manufacturer's instructions and stored at −80 °C for subsequent quantitative real-time PCR (qRT-PCR).

***De novo* assembly and quality assessment**

Fastp v0.20.1 (Chen et al., 2018) was used to filter reads containing adapters and low-quality reads (reads containing *N*>0.002 or >50% bases with a *Q*-value≤20) to acquire clean data to ensure the quality and reliability of data analysis. The clean reads were then assembled into transcripts using Trinity v2.8.5 (Grabherr et al., 2011; Haas et al., 2013) and clustered into unigenes with Corset v1.09 (Davidson & Oshlack, 2014) for hierarchical clustering by removing transcript redundancy and selecting the longest transcripts as unigenes. The quality of the assembled transcripts and unigenes was assessed by evaluating three criteria: i.e., gene coverage, assembly statistics, and ortholog completeness. Gene coverage was calculated by comparing the clean reads from each sample of *N. fuscus*, *L. brandtii*, and *M. musculus* with their assembled transcripts or unigenes. Assembly statistics of transcripts and unigenes of the three species were checked using TrinityStats.pl script, including total number, total assembled bases, average contig length, and N50 and GC content. Ortholog completeness of unigenes was examined using BUSCO v4.0.5 (Simão et al., 2015) against a mammalian database with transcriptome mode. The length distribution of the unigenes was calculated using Perl scripts, which were uploaded to GitHub (https://github.com/lxjbio/Calculate-length-distribution).

Functional annotation of unigenes

The functions of the unigenes were examined by searching the homologous sequences of all unigenes against six public

databases, including the National Center for Biotechnology Information (NCBI) nonredundant database (Nr), Swiss-Prot database, euKaryotic Orthologous Groups (KOG), eggNOG orthology data (EggNOG), Kyoto Encyclopedia of Genes and Genomes (KEGG), and Gene Ontology (GO) database for *N. fuscus, L. brandtii*, and *M. musculus*. For Nr, Swiss-Prot, and KOG annotations, the BLASTX program (BLAST+ suite, v2.9.0) was used to identify putative functions for homologs with an E-value cutoff of $1e^{-5}$, with the best hit retained. For EggNOG annotation, eggnog-mapper v2.0.1 (Huerta-Cepas et al., 2017) was used to identify orthologs with default parameters based on the eggNOG orthology v5.0 database (Huerta-Cepas et al., 2019). For KEGG annotation, KEGG Automatic Annotation Server (KAAS, https://www.genome.jp/kegg/kaas/) was retrieved to obtain KEGG orthology assignments and pathways using the single-directional best-hit method (Batista et al., 2019; Moriya et al., 2007; Zeng et al., 2019). For GO annotation, Blast2GO (Conesa et al., 2005) implemented in OmicsBox v1.3.3 (https://www.biobam.com/omicsbox/) was used to classify unigenes into three categories (biological process, cellular component, and molecular function) to provide a dynamically updated standardized vocabulary for assigning the functions of genes and their products based on the top 20 BLAST results from Swiss-Prot. The distribution of GO function classification for the unigenes was then plotted using OmicShare (https://www.omicshare.com/tools).

Analysis of differential gene expression

Gene expression levels were calculated by mapping the clean reads of *N. fuscus*, *L. brandtii*, and *M. musculus* to their respective unigenes using bowtie2 in the RSEM package (Li & Dewey, 2011). The obtained count value was exported to DESeq2 (Love et al., 2014) for differential expression analysis between the hypoxic and normoxic treatment groups and the resulting *P*-values were adjusted using the Benjamini and Hochberg approach to control for the false discovery rate (FDR). Unigenes with $|\log_2(\text{fold-change})| \geq 1$ and adjusted $P<0.05$ were designated as differentially expressed genes (DEGs). Volcano and heatmap plots of DEGs were drawn using the ggplot2 package and R software, respectively.

Functional enrichment and protein-protein interaction (PPI) analysis

Information regarding DEG functions was collected from unigene annotations and the DEGs were examined using GO and KEGG enrichment analyses to determine potential biological functions and metabolic pathways. The GO and KEGG enrichment analyses were performed using hypergeometric statistical tests, and *P*-values were corrected for multiple testing. GO terms and KEGG pathways with enrichment at $P<0.05$ (modified Fisher's exact test) and more than two genes enriched were considered as significantly enriched functions (Koga et al., 2021; Lavergne et al., 2020; Liu et al., 2015). Hub genes were identified by constructing PPI networks using the Search Tool for the Retrieval of Interacting Genes (STRING) database (https://string-db.org/) with the Markov clustering (MCL) algorithm, and subsequently visualized in Cytoscape v3.8.2 (Shannon et al., 2003).

qRT-PCR analysis and validation

Six genes, including two oxygen transport-associated genes and four randomly selected genes, were chosen for qRT-PCR to verify the reliability of our RNA-seq data and analysis. Primers for qRT-PCR were designed using Oligo7 software and further confirmed online using the Primer-BLAST tool available at NCBI (https://www.ncbi.nlm.nih.gov/tools/primer-blast/). The qRT-PCR procedure was performed in a 25 μL reaction mixture (12.5 μL of UltraSYBR mixture, 0.5 μL of PCR forward primer (10 μmol/L), 0.5 μL of PCR reverse primer (10 μmol/L), 1 μL of template cDNA, and 10.5 μL of ddH_2O) using a LightCycler 480 (Roche Diagnostics, Germany) under the following conditions: polymerase activation at 95 °C for 10 min, followed by 40 cycles of DNA denaturation at 95 °C for 10 s, primer annealing temperature for 30 s, extension at 72 °C for 32 s, and final melt-curve analysis at 95 °C for 15 s, 60 °C for 1 min, 95 °C for 15 s, and 60 °C for 15 s to measure nonspecific PCR products. All qRT-PCR analyses were performed using three biological repeats and three technical repeats to minimize experimental error, and the whole process was performed on ice and in darkness to avoid degradation of experimental samples. Relative gene expression levels were calculated using the $2^{-\Delta\Delta Ct}$ method with β-actin as the internal control (Kashyap et al., 2015; Xu et al., 2019). GraphPad Prism v8.0.1 was used to analyze the relationship between gene expression levels measured by qRT-PCR and RNA-seq using Pearson correlation analysis.

RESULTS

Histological changes in the heart

H&E staining revealed that heart morphology in *N. fuscus* and *L. brandtii* did not change significantly in response to hypoxia, whereas the intercellular spacing between myocardial cells in *M. musculus* increased significantly (Figure 1A–F). Masson staining revealed that collagen fiber content in the *N. fuscus* and *L. brandtii* hearts did not change significantly after exposure to hypoxia but increased significantly in *M. musculus* ($P<0.01$; Figure 1G; Supplementary Figure S1).

Hematological parameters

Among the seven hematological indicators tested, *N. fuscus* showed a significantly lower MCV after hypoxia treatment compared with normoxia treatment ($P<0.05$; Figure 1H). Mice showed significantly higher HCT, MCV, and RDW after hypoxia treatment ($P<0.05$; Figure 1J), whereas *L. brandtii* showed no significant differences in any index in response to hypoxia (Figure 1I).

RNA-seq and assembly

The RNA quality of all samples was assessed using a cutoff RIN value ≥7.5, which showed that the quality of the RNA samples was good (Supplementary Table S1). RNA-seq yielded a total number of 1 035 084 256 paired reads for *N. fuscus*, *L. brandtii*, and *M. musculus* (Supplementary Table S2). After removing the adaptors and filtering low-quality reads, 1 018 238 884 clean reads were retained, with >95.05% Q30 bases in each sample (Supplementary Table S2). *De novo* assembly generated 528 549 transcripts (mean length,

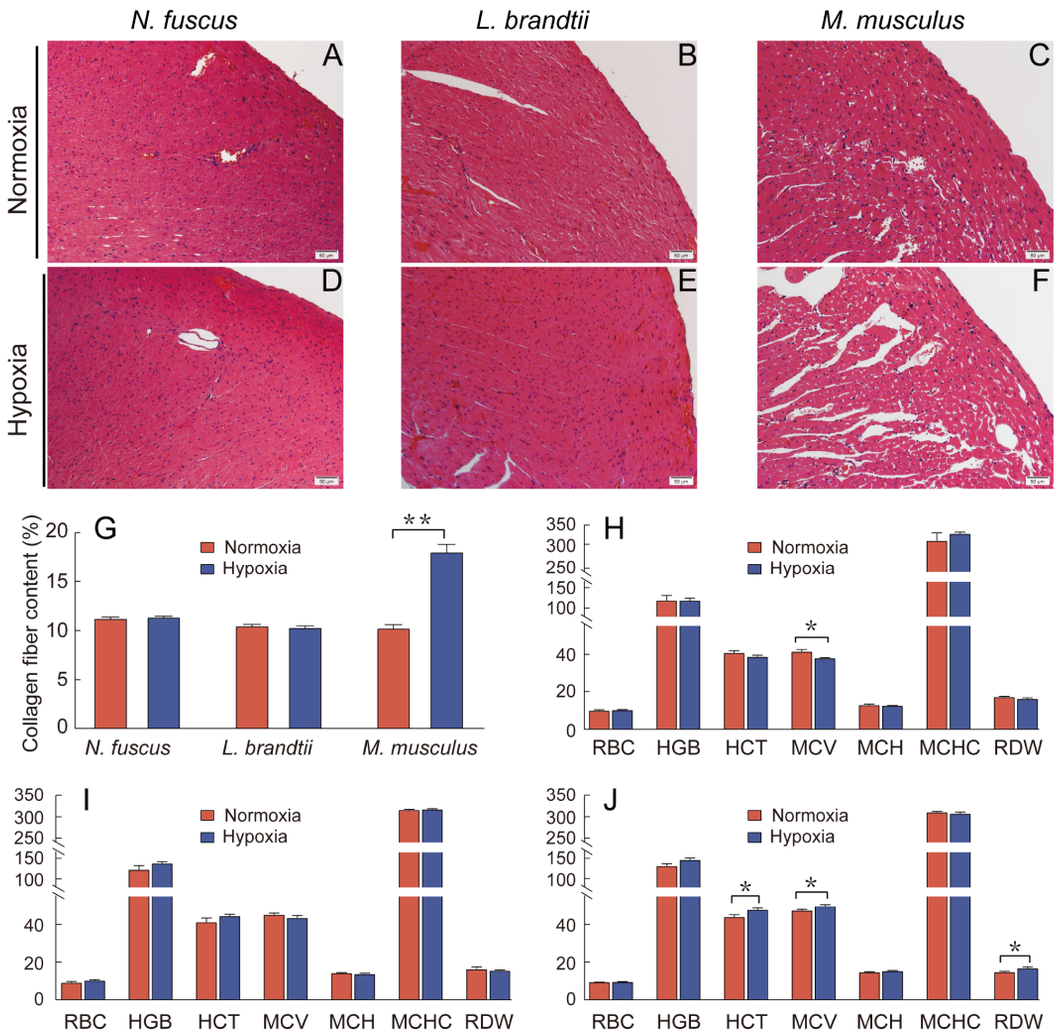

Figure 1 Changes in heart tissue morphology, collagen fiber content, and erythrocyte system before and after hypoxia treatment

A–F: H&E staining of *N. fuscus* (A, D), *L. brandtii* (B, E), and *M. musculus* hearts (C, F). Heart tissue morphology of three species under normoxia (A, B, C) and hypoxia (D, E, F). 200× magnification. G: Changes in collagen fiber content (%) in *N. fuscus*, *L. brandtii*, and *M. musculus* hearts in response to normoxia and hypoxia. H–J: Erythrocyte system parameters in *N. fuscus* (H), *L. brandtii* (I), and *M. musculus* (J) under normoxic and hypoxic conditions. RBC, red blood cells (10^{12}/L); HGB, hemoglobin (g/L); HCT, hematocrit (%); MCV, mean corpuscular volume (fL); MCH, mean red blood cell hemoglobin (pg); MCHC, mean red blood cell hemoglobin concentration (g/L); RDW, red blood cell distribution width (%). *: P<0.05; **: P<0.01.

858.35 bp) hierarchically clustered into 153 192 unigenes (mean length, 1 102.67 bp) in *N. fuscus* with an N50 (minimum contig length required to cover 50% of unigenes) value of 1 748 bp (Table 1). The same method was used to obtain 471 494 transcripts (mean length, 881.75 bp) and 132 299 unigenes (mean length, 1 150.20 bp) with an N50 value of 1 915 bp for *L. brandtii*, and 471 657 transcripts (mean length, 864.98 bp) and 137 036 unigenes (mean length, 1 112.32 bp) with an N50 value of 1 847 bp for *M. musculus* (Table 1). Moreover, the filtered clean reads from each sample were aligned to the transcripts and unigenes with a mapping rate of 92.16% and 87.09%, respectively. The completeness of the unigenes was close to 80% (Table 1) and the main length distribution range of the unigenes ranged from 500 to 1 000 bp in the three species (Supplementary Figure S2A and Table S3).

Functional annotation and classification of unigenes

In *N. fuscus*, *L. brandtii*, and *M. musculus*, 44 404 (28.99%), 41 384 (31.28%), and 45 967 (33.54%) unigenes, respectively, were annotated in at least one of the six databases (Supplementary Table S4), and 15 589, 15 701, and 15 140 unigenes, respectively, were assigned to all six databases (Supplementary Figure S2B–D). For *N. fuscus*, *L. brandtii*, and *M. musculus*, Nr annotation identified 39 110 (25.53%), 37 302 (28.20%), and 41 306 (30.14%) unigenes, respectively, with homologous proteins (Supplementary Figure S2 and Table S4). Swiss-Prot annotation identified 33 455 (21.84%), 32 025 (24.21%), and 33 001 (24.08%) unigenes, respectively, with homologous proteins (Supplementary Figure S2 and Table S4). For KOG analysis, 24 113 (15.74%), 23 124 (17.48%), and 23 144 (16.89%) unigenes, respectively, were assigned to 25 functional classifications (Supplementary Figures S2, S3

Table 1 Transcriptome assembly metrics and assessment results in *N. fuscus*, *L. brandtii*, and *M. musculus*

Assembly metric	*N. fuscus*	*L. brandtii*	*M. musculus*
Total number of Trinity transcripts (*n*)	528 549	471 494	471 657
Total assembled bases of transcripts (bp)	453 677 736	415 739 886	407 973 875
Mean length of transcripts (bp)	858.35	881.75	864.98
N50 of transcripts (bp)	2 483	2 566	2 530
GC content of transcripts (%)	47.69	47.82	47.80
Mapping rate to transcripts (%)	92.54–93.78	92.61–93.55	92.16–93.81
Total number of unigenes (*n*)	153 192	132 299	137 036
Total assembled bases of unigenes (bp)	168 920 719	152 170 285	152 428 218
Mean length of unigenes (bp)	1 102.67	1 150.20	1 112.32
N50 of unigenes (bp)	1 748	1 915	1 847
GC content of unigenes (%)	46.90	47.12	47.07
Mapping rate to unigenes (%)	88.36–90.19	88.61–89.33	87.09–88.84
BUSCO completeness of unigenes (%)	80.4	79.2	80.8

and Table S4). For GO annotation, 28 280 (18.46%), 27 838 (21.04%), and 27 480 (20.05%) unigenes, respectively, were assigned to one or more terms of the three categories (Supplementary Figures S2, S4 and Table S4).

DEG identification

Comparative transcriptome analysis was performed between the normoxia and hypoxia treatment groups to identify DEGs in response to hypoxic stress. As a result, 788 DEGs were identified in *N. fuscus*, including 286 up-regulated and 502 down-regulated genes (Supplementary Figure S5A), among which, 71 up-regulated and 119 down-regulated genes were annotated (Supplementary Tables S5, S6). Likewise, 572 DEGs were identified in *L. brandtii*, including 267 up-regulated and 305 down-regulated genes (Supplementary Figure S5B), among which 75 up-regulated and 117 down-regulated genes were annotated (Supplementary Tables S5, S6). In addition, 1 297 DEGs were identified in *M. musculus*, including 831 up-regulated and 466 down-regulated genes (Supplementary Figure S5C), among which 244 up-regulated and 136 down-regulated genes were annotated (Supplementary Tables S5, S6). Furthermore, cluster analysis of the DEGs showed that the three biological replicates in the normoxia and hypoxia treatment groups were clustered together for each species (Supplementary Figure S5D–F).

Functional enrichment analysis of DEGs

In *N. fuscus*, the up-regulated DEGs were significantly enriched in 120 GO terms, including 112 biological process terms, five cellular component terms, and three molecular function terms (Figure 2A; Supplementary Table S7). These enriched terms were mainly related to cellular processes (single-organism cellular process, transport, establishment of localization, cell differentiation, localization, cell morphogenesis, cellular developmental process, cellular component morphogenesis, and cell morphogenesis involved in differentiation), development (blood vessel morphogenesis, blood vessel development, and vasculature development), and signal transduction (negative regulation of signal transduction, negative regulation of signaling, positive regulation of signal transduction, positive regulation of signaling, regulation of signal transduction, and regulation of signaling). The down-regulated DEGs were only significantly enriched in seven GO molecular function terms (Figure 2B; Supplementary Table S7), which were all related to binding activity (ion binding, nucleic acid binding transcription factor activity, transcription factor activity, sequence-specific DNA binding, protein binding, bridging, binding, bridging, lipid binding, and DNA binding).

In *L. brandtii*, the up-regulated DEGs were significantly enriched in 31 GO terms, including 24 biological process terms, five cellular component terms, and two molecular function terms (Figure 3A; Supplementary Table S7). Most enriched GO terms were related to stimulus and regulation (response to stimulus, regulation of biological quality, homeostatic process, and biological regulation), cellular processes (transport, establishment of localization, localization, plasma membrane organization, endomembrane system organization, single-organism membrane organization, membrane, cytoskeleton organization, multicellular organismal process, single-organism cellular process, cell differentiation, intracellular, and cytoplasm), development (single-organism developmental process, developmental process, and anatomical structure development), and enzyme activity (oxidoreductase activity). The down-regulated DEGs were significantly enriched in 42 GO terms, including 20 biological process terms, 13 cellular component terms, and nine molecular function terms (Figure 3B; Supplementary Table S7). The enriched terms were mainly related to metabolic process (small molecule metabolic process, single-organism metabolic process, lipid metabolic process, catabolic process, cellular amino acid metabolic process, organic acid metabolic process, carboxylic acid metabolic process, oxoacid metabolic process, secondary metabolic process, nitrogen cycle metabolic process, and cofactor metabolic process, and other terms) and enzyme activity (mitochondrion, oxidoreductase activity, catalytic activity, transferase activity, lyase activity, isomerase activity, and enzyme regulator activity).

In *M. musculus*, the up-regulated DEGs were significantly enriched in 28 GO terms, including 15 biological process terms, nine cellular component terms, and four molecular function terms (Figure 4A; Supplementary Table S7). Most enriched GO terms were related to stimulus and regulation response of stimulation (response to stress, response to

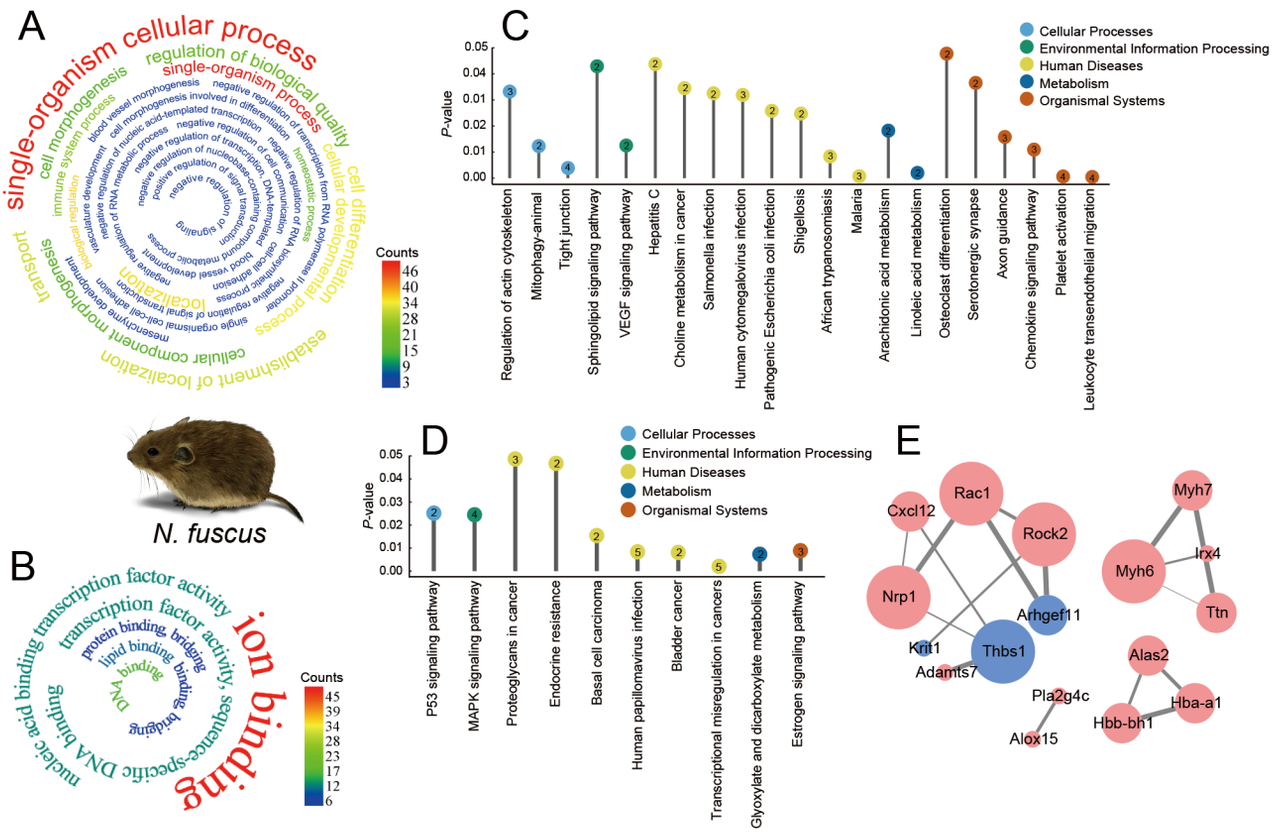

Figure 2 GO enrichment, KEGG enrichment, and PPI results for up-regulated and down-regulated DEGs in *N. fuscus*

A, B: Different colors represent number of genes significantly enriched in GO terms (see color key) and font size represents *P*-value significance level (larger font indicates smaller *P*). Top 30 significantly enriched GO terms in up-regulated DEGs are shown in Figure A, and all significantly enriched GO terms are presented in Supplementary Table S7. C, D: Different-colored circles represent different biological classifications (see color key) and numbers in circles represent number of genes significantly enriched in KEGG pathways. E: Red and blue circles represent proteins encoded by up-regulated and down-regulated DEGs, respectively. Circle size represents number of other proteins in network that interact with that protein, with larger circles indicating greater number of proteins interacting with protein in question. Thickness of line connecting circles indicates strength of interaction between two proteins, with wider lines indicating stronger interaction.

stress, and response to stimulus), metabolic process (metabolic process, cellular protein metabolic process, protein metabolic process, and sulfur compound metabolic process), cellular processes (cellular macromolecular complex assembly, cell adhesion, and aging), and enzyme activity (isomerase activity and enzyme regulator activity). The down-regulated DEGs were significantly enriched in 12 GO terms, including eight biological process terms, two cellular component terms, and two molecular function terms (Figure 4B; Supplementary Table S7). These enriched terms were mainly related to cell process (cell proliferation, multicellular organismal process, single-multicellular organism process, protein maturation, aging, and extracellular region), development (embryo development, multicellular organism development, and single-organism developmental process), and enzyme activity (enzyme regulator activity).

Metabolic pathway enrichment analysis of DEGs

In *N. fuscus*, the up-regulated DEGs were significantly enriched in 21 pathways related to cellular processes (regulation of actin cytoskeleton, mitophagy-animal, and tight junction), environmental information processing (sphingolipid signaling pathway and vascular endothelial growth factor (VEGF) signaling pathway), human disease (hepatitis C, choline metabolism in cancer, salmonella infection, human cytomegalovirus infection, pathogenic *Escherichia coli* infection, shigellosis, African trypanosomiasis, and malaria), metabolism (arachidonic acid metabolism and linoleic acid metabolism), and organismal systems (osteoclast differentiation, serotonergic synapse, axon guidance, chemokine signaling pathway, platelet activation, and leukocyte transendothelial migration) (Figure 2C; Supplementary Table S8). The down-regulated DEGs were significantly enriched in 10 pathways related to cellular processes (P53 signaling pathway), environmental information processing (MAPK signaling pathway), human disease (proteoglycans in cancer, endocrine resistance, basal cell carcinoma, human papillomavirus infection, bladder cancer, and transcriptional misregulation in cancers), metabolism (glyoxylate and dicarboxylate metabolism), and organismal systems (estrogen signaling pathway) (Figure 2D; Supplementary Table S8).

In *L. brandtii*, the up-regulated DEGs were significantly

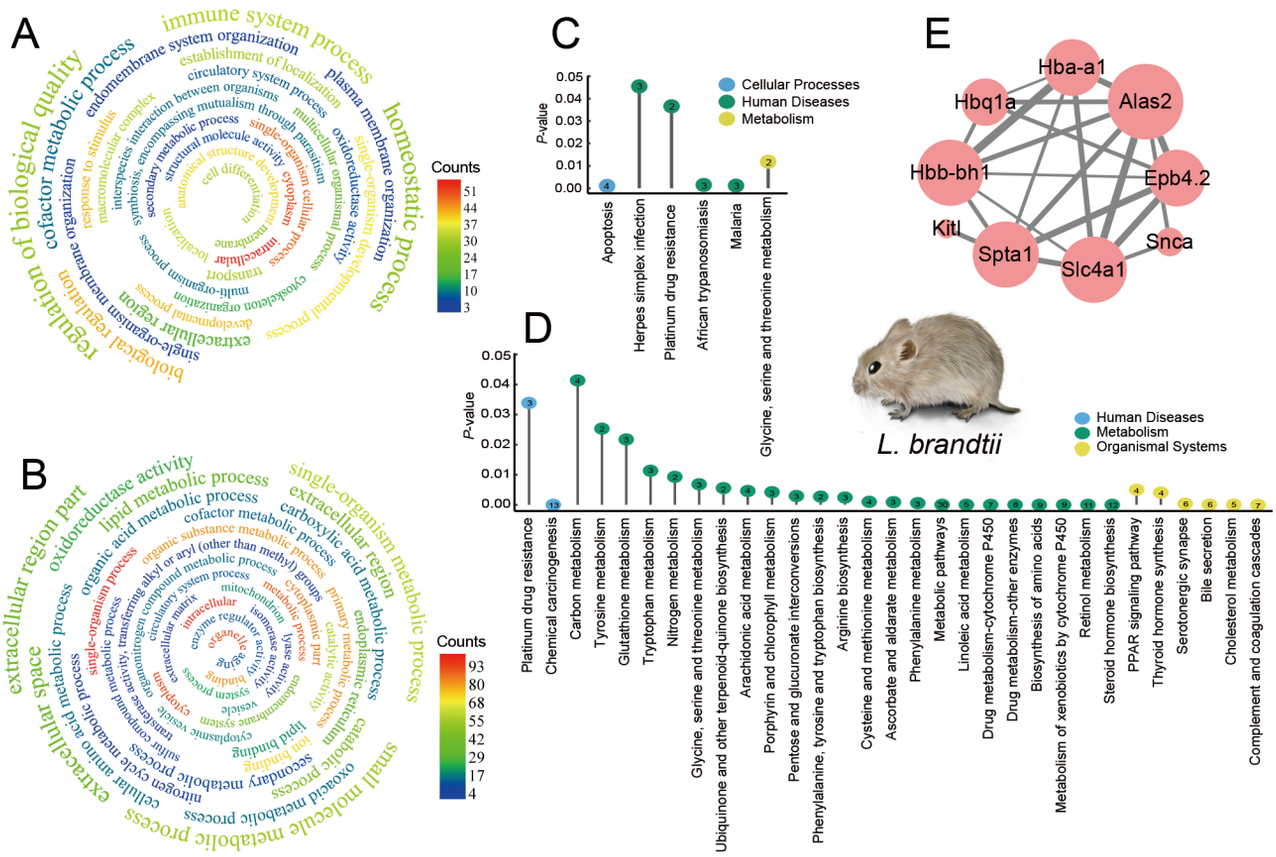

Figure 3 GO enrichment, KEGG enrichment, and PPI results for up-regulated and down-regulated DEGs in *L. brandtii*

A, B: Different colors represent number of genes significantly enriched in GO terms (see color key) and font size represents *P*-value significance level (larger font indicates smaller *P*). C, D: Different-colored circles represent different biological classifications (see color key) and numbers in circles represent number of genes significantly enriched in KEGG pathways. E: Red and blue circles represent proteins encoded by up-regulated and down-regulated DEGs, respectively. Circle size represents number of other proteins in network that interact with that protein, with larger circles indicating greater number of proteins that interact with protein in question. Thickness of line connecting circles indicates strength of interaction between two proteins, with wider lines indicating stronger interaction.

enriched in six pathways related to cellular processes (apoptosis), human disease (herpes simplex infection, platinum drug resistance, African trypanosomiasis, and malaria), and metabolism (glycine, serine, and threonine metabolism) (Figure 3C; Supplementary Table S8). The down-regulated DEGs were significantly enriched in 31 pathways related to human disease (platinum drug resistance and chemical carcinogenesis), metabolism (carbon metabolism, tyrosine metabolism, glutathione metabolism, tryptophan metabolism, nitrogen metabolism, glycine, serine, and threonine metabolism, ubiquinone and other terpenoid-quinone biosynthesis, arachidonic acid metabolism, porphyrin and chlorophyll metabolism, pentose and glucuronate interconversions, phenylalanine, tyrosine, and tryptophan biosynthesis, arginine biosynthesis, cysteine and methionine metabolism, ascorbate and aldarate metabolism, phenylalanine metabolism, metabolic pathways, linoleic acid metabolism, drug metabolism-cytochrome P450, drug metabolism-other enzymes, biosynthesis of amino acids, metabolism of xenobiotics by cytochrome P450, retinol metabolism, and steroid hormone biosynthesis), and organismal systems (PPAR signaling pathway, thyroid hormone synthesis, serotonergic synapse, bile secretion, cholesterol metabolism, and complement and coagulation cascades) (Figure 3D; Supplementary Table S8).

In *M. musculus*, the up-regulated DEGs were significantly enriched in 14 pathways related to cellular processes (autophagy-animal, p53 signaling pathway, and autophagy-other eukaryotes), environmental information processing (apelin signaling pathway and Jak-STAT signaling pathway), human disease (pancreatic cancer, platinum drug resistance, and human cytomegalovirus infection), metabolism (propanoate metabolism, tyrosine metabolism, valine, leucine, and isoleucine degradation, metabolic pathways, and nicotinate and nicotinamide metabolism), and organismal systems (PPAR signaling pathway) (Figure 4C; Supplementary Table S8). The down-regulated DEGs were significantly enriched in 14 pathways related to cellular processes (focal adhesion, adherens junction, tight junction, and apoptosis), environmental information processing (hippo signaling pathway), human disease (bladder cancer, microRNAs in cancer, thyroid cancer, proteoglycans in cancer,

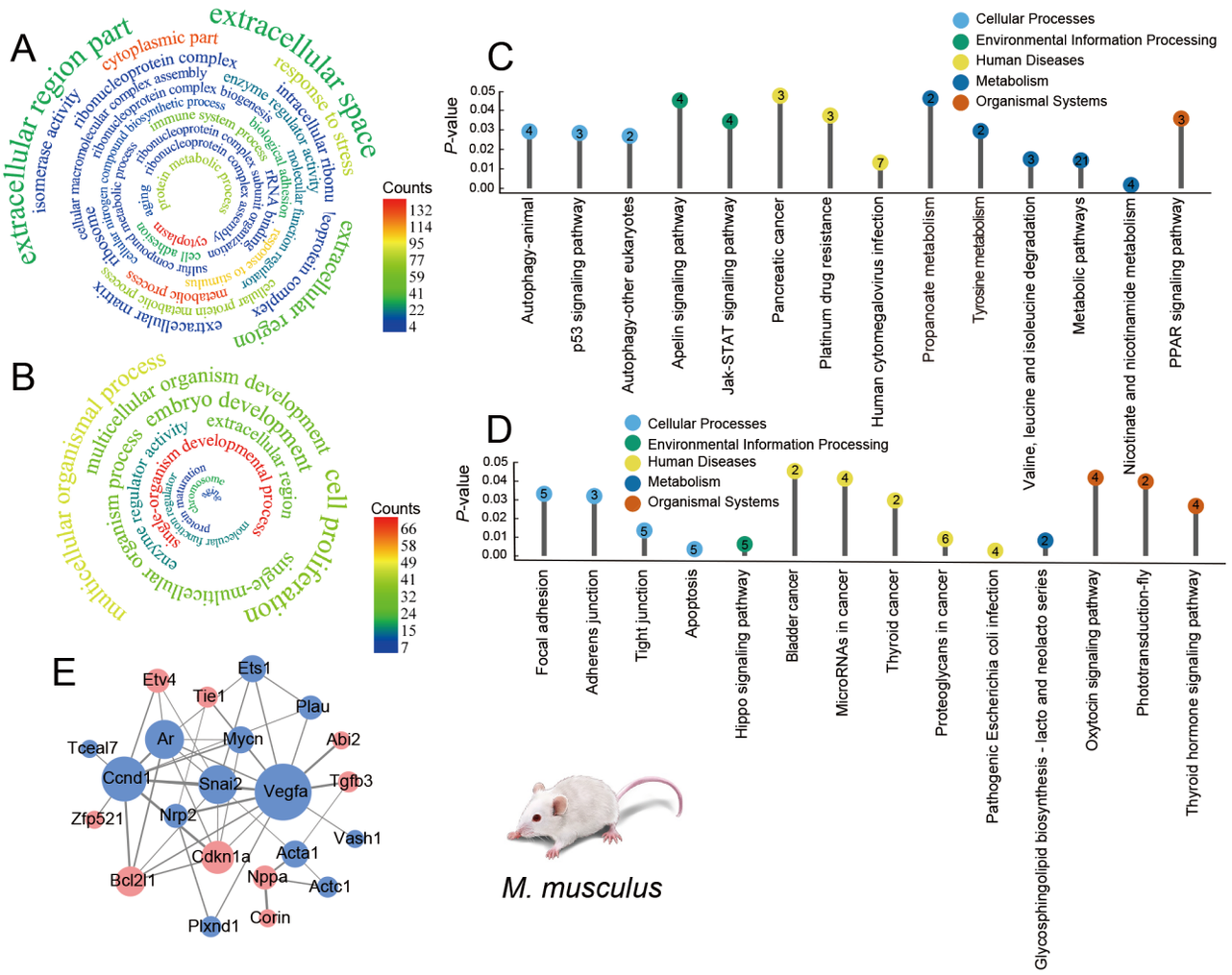

Figure 4 GO enrichment, KEGG enrichment, and PPI results for up-regulated and down-regulated DEGs in *M. musculus*

A, B: Different colors represent number of genes significantly enriched in GO terms (see color key) and font size represents *P*-value significance level (larger font indicates smaller *P*). C, D: Different-colored circles represent different biological classifications (see color key) and numbers in circles represent number of genes significantly enriched in KEGG pathways. E: Red and blue circles represent proteins encoded by up-regulated and down-regulated DEGs, respectively. Circle size represents number of other proteins in network that interact with that protein, with larger circles indicating greater number of proteins that interact with protein in question. Thickness of line connecting circles indicates strength of interaction between two proteins, with wider lines indicating stronger interaction.

and pathogenic *Escherichia coli* infection), metabolism (glycosphingolipid biosynthesis-lacto and neolacto series), and organismal systems (oxytocin signaling pathway, phototransduction-fly, and thyroid hormone signaling pathway) (Figure 4D; Supplementary Table S8).

Validation of RNA-seq results by qRT-PCR

All qRT-PCR experiments were performed using specific primers for amplification of target genes (Supplementary Table S9). The expression profiles of six genes, including *Hba* and *Alas2*, which are involved in oxygen transport, showed a similar trend (Figure 5A–C) and were highly significantly correlated (R^2=0.9676, P<0.01 for *N. fuscus*, R^2=0.9802, P<0.01 for *L. brandtii*, and R^2=0.9581, P<0.01 for *M. musculus*; Figure 5D–F) to the RNA-seq assay, indicating the reliability of our transcriptome analysis.

DISCUSSION

Hypoxia can disrupt homeostasis and lead to impaired cardiac function and even death in many organisms, including humans. Studying the hypoxic response mechanism of the cardiovascular system in animals that have adapted to such environments can provide valuable information for the protection of humans and other animals. In the present study, we assessed the response and regulation of the cardiovascular system to hypoxia in two closely related rodents, *N. fuscus* and *L. brandtii*, and used *M. musculus* for comparison. Compared with the mice, *N. fuscus* and *L. brandtii* exhibited a strong tolerance to hypoxia, but via different adaptation mechanisms.

Physiological response to hypoxia

Histological analysis revealed that the cardiac tissue

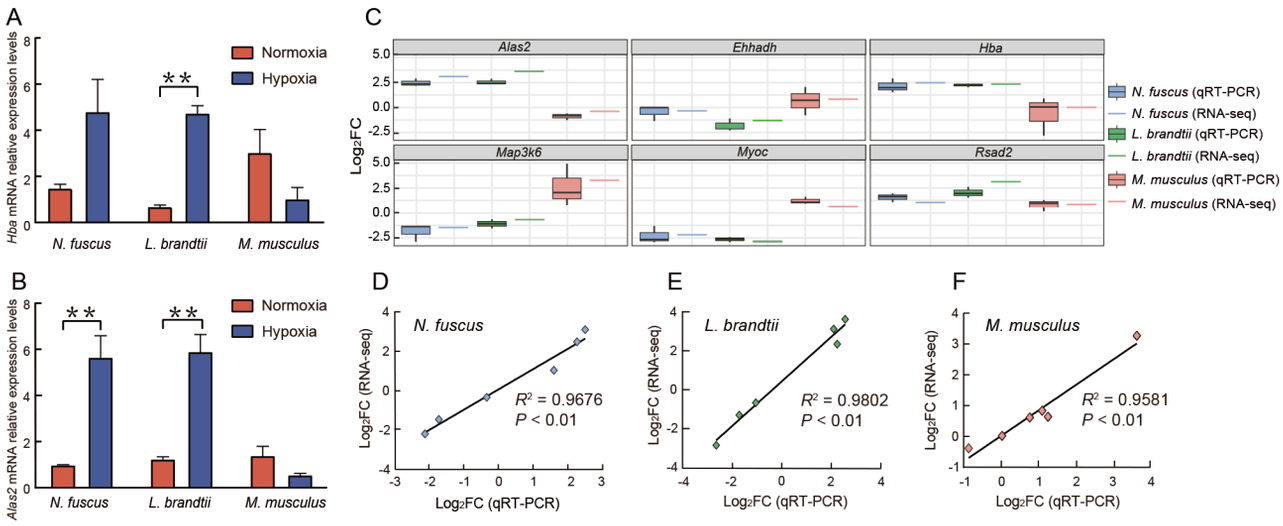

Figure 5 Gene expression levels measured by qRT-PCR and RNA-seq methods

A, B: Relative expression levels of *Hba* (A) and *Alas2* (B) in *N. fuscus*, *L. brandtii*, and *M. musculus*. C–F: Gene expression trends (C) and correlations (D–F) of six genes between qRT-PCR and RNA-seq in *N. fuscus*, *L. brandtii*, and *M. musculus*.

morphology and collagen fiber content of *N. fuscus* and *L. brandtii* did not change significantly in response to hypoxia compared with normoxia (Figure 1; Supplementary Figure S1), indicating a strong tissue-level tolerance to hypoxia. However, in *M. musculus*, myocardial cell spacing and tissue fibrosis increased significantly, indicating that external hypoxia caused tissue damage (Figure 1; Supplementary Figure S1). Hematological analysis revealed that MCV was significantly reduced in *N. fuscus* under hypoxic conditions, which may help decrease blood viscosity, reduce blood circulation resistance, and facilitate oxygen diffusion in hypoxic environments (Kong et al., 2019; Verghese, 2013). In contrast, MCV and HCT were significantly increased in *M. musculus*, consistent with previous study (Liu et al., 2010; Roklicer et al., 2020), which may increase blood circulation resistance. In addition, RDW was also significantly increased in *M. musculus*, which can rapidly increase in response to RBC rupture. Notably, increased RDW is significantly negatively correlated with RBC deformation and may increase cardiac load and cardiovascular disease (Yoon et al., 2015). The elevation of these three blood parameters in *M. musculus* may be due to hypoxia promoting erythropoietin production, thereby inducing the formation of enlarged RBCs (Yčas et al., 2015).

Transcriptome response to hypoxia

Enhanced oxygen transport efficiency in *N. fuscus* and *L. brandtii* under hypoxia: Results showed that *N. fuscus* and *L. brandtii* coped with hypoxia by enhancing oxygen transport efficiency, and this functional convergence appears to be due to varied gene regulation patterns. *Myh6* and *Myh7*, two key genes encoding αMyHC and βMyHC proteins, respectively, were significantly up-regulated in the *N. fuscus* heart under hypoxic conditions (Figures 2E, 6; Supplementary Table S6). High expression of these genes in mammals is associated with accelerated cardiac contraction and economical contractility (Grimes et al., 2017; Miyata et al., 2000; Yin et al., 2015). Therefore, we speculate that the significant increase in *Myh6* and *Myh7* may enhance cardiac contractility in *N. fuscus* in hypoxic conditions and improve oxygen transport efficiency. In addition to the up-regulation of genes involved in cardiac contraction, genes related to angiogenesis and endothelial cell proliferation were also significantly up-regulated (*Rac1*, *Pla2g4c*, *Alox15*, *Nrp1*, *Cxcl12*, *Rock2*, and *Notch4*) or down-regulated (*Krit1*, *Thbs1*, and *Angptl7*) in *N. fuscus* under hypoxic conditions, with most genes enriched in the VEGF signaling pathway, blood vessel morphogenesis, blood vessel development, vasculature development, and other pathways (Figures 2, 6; Supplementary Table S6). Among these genes, *Rac1* plays an important role in regulating the proliferation and migration of vascular smooth muscle cells and the rearrangement of endothelial cells (Sawada et al., 2010). Significant up-regulation of *Pla2g4c* and *Alox15* promotes the release of arachidonic acid, which, in turn, promotes prostaglandin production, thereby promoting angiogenesis (Barnett et al., 2010; Singh & Rao, 2019). Significant up-regulation of *Nrp1*, *Cxcl12*, *Rock2*, and *Notch4* may also have promoted angiogenesis and vascular development in *N. fuscus* to some extent (He et al., 2010; Kryczek et al., 2005; Mehta et al., 2018; Trindade & Duarte, 2020). In agreement, we also found significant down-regulation in *Krit1*, *Thbs1*, and *Angptl7*, which encode antiangiogenic proteins (Figures 2E, 6; Supplementary Table S6) and negatively regulate angiogenesis (Lawler, 2002; Orso et al., 2013; Toyono et al., 2015). Based on these findings, we speculate that *N. fuscus* may promote angiogenesis *in vivo* via a complex network of multiple genes, thereby enhancing blood circulation and facilitating oxygen transport under hypoxic conditions.

Spta1, *Slc4a1*, and *Epb42* were significantly up-regulated in *L. brandtii* under hypoxic conditions and strongly interacted with *Hba* and *Hbb* (Figure 3E; Supplementary Table S10). Of note, these three genes encode spectrin, band 3, and protein 4.2, respectively, which are important skeletal proteins in the erythrocyte membrane (Cox et al., 2019; Long et al., 2015; Schneider et al., 2009; Wang et al., 2017a; Wu et al., 2019).

Therefore, the synergistic and significant up-regulation of *Spta1*, *Slc4a1*, and *Epb42* may help *L. brandtii* maintain stable erythrocyte morphology *in vivo* under hypoxic conditions to ensure oxygen supply (Figure 6). Band 3 also acts as a transporter to mediate electron neutralization and anion exchange in the cell membrane, promoting the exchange of chloride and bicarbonate on the erythrocyte plasma membrane and the elimination of carbon dioxide from tissues (Arakawa et al., 2015). *Bpgm*, which encodes an allosteric regulator of hemoglobin, was up-regulated in response to hypoxia (Supplementary Table S6). This gene promotes the release of oxygen by regulating the affinity of O_2 and hemoglobin when blood flows through tissues (Sun et al., 2016).

In addition to different regulatory mechanisms, we also identified synchronized gene expression regulation shared by *N. fuscus* and *L. brandtii*. For example, the expression levels of *Hba* and *Hbb*, which encode the α-globin and β-globin subunits for hemoglobin, respectively, were significantly up-regulated in both species (Figures 2E, 3E, 6 and Supplementary Table S6). Hemoglobin is the main respiratory protein in mammalian RBCs and plays a central role in binding and transporting oxygen to support the energy and metabolic requirements essential for life (Zhang et al., 2015). Species living in hypoxic environments for prolonged periods have shown an increase in the ability of hemoglobin to absorb and transport oxygen by up-regulating the expression of *Hba* and *Hbb in vivo* (Dong et al., 2018; Yang et al., 2018). Here, PPI analysis showed a strong synergistic up-regulation in *Alas2*, *Hba*, and *Hbb* in both *N. fuscus* and *L. brandtii* (Figures 2E, 3E; Supplementary Table S10). *Alas2*, which encodes 5-aminolevulinic acid synthase 2 in erythroid cells, synthesizes heme for hemoglobin (Abu-Farha et al., 2005) and its up-regulation increases heme content in RBCs (Hofer et al., 2003; Khechaduri et al., 2013). Heme binds to globin subunits encoded by *Hba* and *Hbb* to form hemoglobin subunits, with the two hemoglobin α and two hemoglobin β subunits then forming adult hemoglobin with heterotetramers to transport oxygen (Brown et al., 2016; Ludwig et al., 2016). Therefore, we speculate that *N. fuscus* and *L. brandtii* maintain sufficient oxygen supply to various tissues and organs under hypoxic conditions via the coordinated regulation of *Hba*, *Hbb*, and *Alas2*.

Mus musculus mice do not reside in hypoxic environments and lack effective oxygen transport strategies to respond to hypoxia. In terms of myocardial contraction, *Acta1* and *Actc1*, which encode alpha-cardiac actin and alpha-skeletal actin, respectively, were significantly down-regulated (Figure 4E; Supplementary Table S6). These two genes are closely linked to myocardial contraction and cardiomyocyte apoptosis (Bildyug, 2019; Frade et al., 2013; Ilkovski et al., 2005). *Nppa* and *Corin* were also significantly up-regulated in *M. musculus* under hypoxic conditions and strongly interacted with *Acta1* and *Actc1* (Figure 4E; Supplementary Table S6). Increased expression of *Nppa* and *Corin* is significantly correlated with physiological and pathological reactions, such as hypoxia, hypertension, myocardial ischemia, ventricular hypertrophy, and heart failure (Xu-Cai & Wu, 2010; Yan et al., 2000). These findings are contrary to the enhanced myocardial contraction characteristics found in *N. fuscus* under hypoxic conditions, thus highlighting the differences in tolerance to hypoxia in these two species. We also identified a series of angiogenesis-related genes (*Nrp2*, *Snail2*, *Ets1*, *Plau*, and *Vash1*) that interacted with *Vegfa* and were significantly down-regulated in *M. musculus* in response to hypoxia (Figure 4E; Supplementary Table S6), which is not conducive to the formation of blood vessels (Boosani and Sudhakar, 2011; Cheng et al., 2019; Lv et al., 2014; Sindi et al., 2020; Zheng et al., 2013).

Context-dependent cardiometabolic strategies in *N. fuscus* and *L. brandtii* under hypoxia: In *N. fuscus*, cardiac metabolism under hypoxic conditions underwent a metabolic shift from fatty acid to glucose oxidation (Figure 7A), with 11 down-regulated genes significantly enriched in lipid binding (Figure 2B; Supplementary Table S7). Among these down-regulated genes, *Acot11* encodes acyl-CoA thioesterases, which catalyze the hydrolysis of long-chain fatty acyl-CoAs to form free fatty acids. Down-regulation of this gene may reduce fatty acid synthesis (Diessler et al., 2018; Jeckel et al., 2014). The down-regulation of *Acss2* was significantly enriched in ion binding and glyoxylate and dicarboxylate metabolism (Supplementary Tables S7, S8). *Acss2* plays an important role in catalyzing acetyl-CoA production during fatty acid oxidation and a significant down-regulation of this gene can result in a

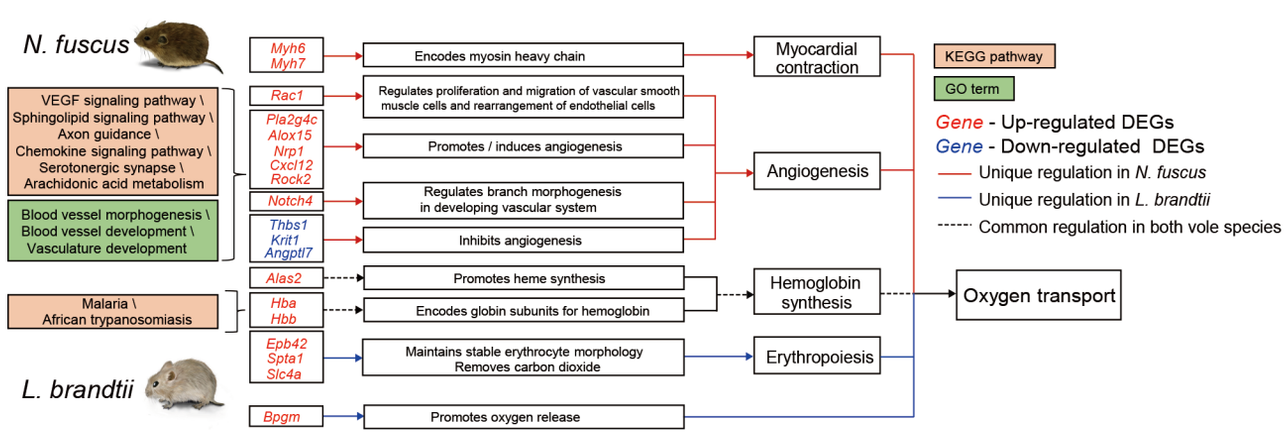

Figure 6 Dynamic deduction of oxygen transport regulation in *N. fuscus* and *L. brandtii* under hypoxic conditions

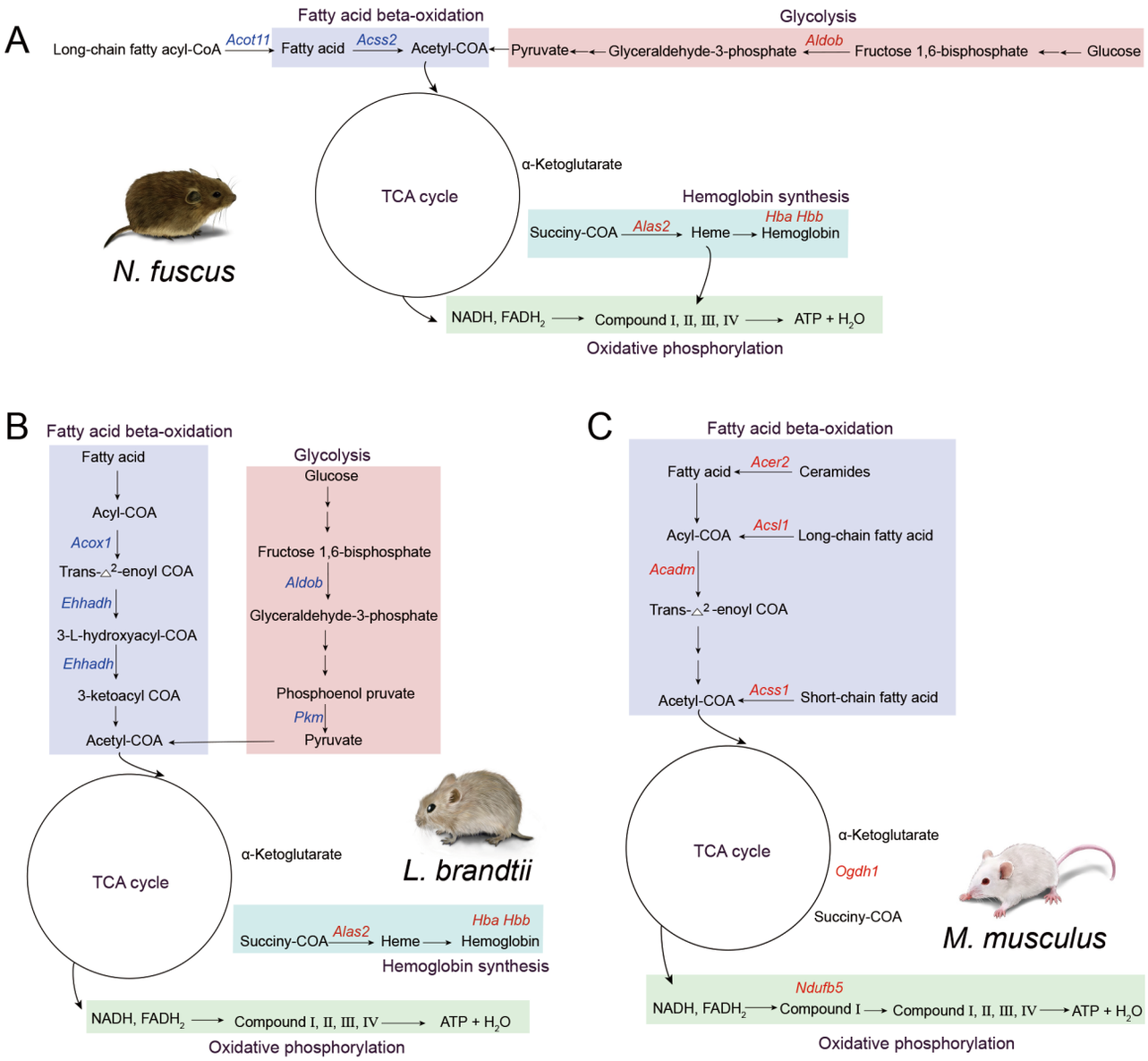

Figure 7 Cardiac energy metabolism pathways activated under hypoxic environments

A: *N. fuscus*. B: *L. brandtii*. C: *M. musculus*. Black arrow represents direction of biochemical reaction, and gene names in red and blue italics represent up-regulated and down-regulated DEGs, respectively.

significant reduction in acetyl-CoA (Martínez-Micaelo et al., 2016; Sun et al., 2018). In contrast to the significant down-regulation of genes related to fatty acid oxidation, we observed a significant up-regulation in *Aldob*, a core gene related to glucose oxidation, in *N. fuscus* under hypoxic conditions (Figure 7A). *Aldob* encodes aldolase B (also known as fructose-bisphosphate aldolase B), a key glycolytic enzyme in vertebrates that catalyzes the conversion of fructose 1,6-bisphosphate to glyceraldehyde 3-phosphate, which is further catabolized to pyruvate (Miller et al., 2012; Pamidimukkala et al., 2018; Potter et al., 2021). Pyruvate is converted into acetyl CoA, which drives the tricarboxylic acid (TCA) cycle and thus energy production via oxidative phosphorylation (Kurniawan et al., 2020). Heme is an indispensable prosthetic group of complex III and complex IV and increased synthesis can promote oxidative phosphorylation (Brennan et al., 2014; Shinzawa-Itoh et al., 2016).

In the adult mammalian heart, more than 70% of adenosine triphosphate (ATP) is produced by oxidation of fatty acids and the remaining is generated by carbohydrates (Hsiao et al., 2021; Peoples et al., 2019). However, under conditions of normal oxygen consumption, carbohydrates (glucose) can produce more ATP than fatty acids, as glucose has higher oxidation efficiency (Bai et al., 2021; Lorenzo et al., 2013). The conversion of animal cardiometabolic substrates from fatty acids to glucose under hypoxic conditions is considered an oxygen-saving strategy, which can improve cardiometabolic efficiency and maintain ATP production (Abdurrachim et al., 2015; Duan et al., 2021; Su et al., 2021). In high-altitude Andean mice, cardiac metabolism promotes

glucose oxidation by increasing the activity of hexokinase as a strategy to conserve oxygen compared with low-altitude counterparts (Schippers et al., 2012). Similarly, based on transcriptome analysis, genes involved in glycolysis are up-regulated in Tibetan pigs compared with Yorkshire pigs, suggesting that glycolysis may be more active in Tibetan pigs to reduce oxygen demand and maintain energy production (Duan et al., 2021). Furthermore, ^{31}P magnetic resonance spectroscopy of high-altitude humans (Sherpas) reveals metabolic organization of the heart to preferentially use carbohydrates (glucose) instead of fatty acids (Hochachka et al., 1996). Even though shifting the "fuel source" from fatty acid to glucose oxidation may be advantageous under hypoxia, it also has disadvantages, such as cardiac hypertrophy (Kolwicz et al., 2012; Ma et al., 2019). Hence, increasing the ratio of glucose oxidative energy in heart tissue may be an important adaptation strategy employed by *N. fuscus* living in hypoxic conditions to maintain an efficient energy supply.

Unlike *N. fuscus*, *L. brandtii* reduced both fatty acid and glucose oxidation in the heart under hypoxic conditions (Figure 7B). In terms of glucose metabolism, *Aldob* expression, which was significantly up-regulated in *N. fuscus*, was significantly down-regulated in *L. brandtii*, thereby inhibiting the conversion of fructose 1,6-bisphosphate to glyceraldehyde 3-phosphate. *Pkm*, which encodes pyruvate kinase, was also significantly down-regulated (Figure 7B; Supplementary Table S6), thus inhibiting the production of pyruvate and ATP from phosphoenolpyruvate (Fan et al., 2019). Changes in fatty acid oxidation included the significant down-regulation of two key genes, *Acox1* and *Ehhadh*, which catalyze the conversion of acyl-CoA to 3-ketoacyl-CoA (Figure 7B; Supplementary Table S6), thus inhibiting fatty acid oxidation in *L. brandtii* (Chen et al., 2016; Qu et al., 2019). Interestingly, under hypoxic conditions, the *L. brandtii* hearts showed significant down-regulation of *Popdc2* (Supplementary Table S6), which is highly expressed in cardiac pacing and conduction systems and plays an important regulatory role in heart rate dynamics (Froese et al., 2012; Milanesi et al., 2015). No or low expression of *Popdc2* in the heart can cause severe arrhythmia and sinus arrest symptoms, which can reduce the average heart rate and lead to a bradycardia phenotype (Froese et al., 2012; Schindler & Brand, 2016). Bradycardia and insufficient cardiac energy supply may affect exercise performance in *L. brandtii* under hypoxic environments, with previous studies showing that nerve synapse excitability and athletic ability are significantly reduced in *L. brandtii* under hypoxic conditions (Dong et al., 2018). Previous studies have also reported that low heart and metabolic rates are common strategies to conserve oxygen in hypoxia-tolerant species (Arieli et al., 1986; Grimes et al., 2017; Kirby et al., 2018; Pamenter et al., 2018). *Lasiopodomys brandtii* voles face hypoxic conditions when resting in their tunnels, with low-level exercise and energy requirements. Therefore, we speculate that appropriate down-regulation of heart rate and energy supply may be an adaptive mechanism to conserve energy consumption under hypoxic conditions (Grimes et al., 2014; Kirby et al., 2018).

In contrast to *N. fuscus* and *L. brandtii*, the *M. musculus* hearts did not exhibit an enhanced glucose oxidation energy supply ratio or a decreased heart rate in relation to reduced energy consumption under hypoxic conditions, and cardiac energy supply was mainly dependent on fatty acid oxidation, consistent with its main source of energy in normoxic conditions (Figure 7C). The mice showed significant up-regulation of four fatty acid oxidation-related genes, including *Acer2*, *Acsl1*, *Acss1*, and *Acadm*, which are involved in catalyzing ceramides, long-chain fatty acids, and short-chain fatty acids to produce intermediate products in the beta-oxidation of fatty acids (Chen et al., 2014; Li et al., 2018; Paul et al., 2014; Wang et al., 2017b). Nevertheless, a single, inflexible energy supply and inadequate substrate oxygen may result in an insufficient cardiac energy supply in *M. musculus* under hypoxia, thereby limiting its survival under these conditions.

Based on the above, our findings suggest that the two vole species exhibit differences in oxygen transport and energy utilization strategies in response to hypoxia, which is, to some extent, corroborated by previous studies in other animals. For example, bar-headed geese cope with the hypobaric and hypoxic conditions encountered when flying over the Himalayas by increasing cardiac output (Scott et al., 2015), while other animals that live in hypoxic environments, such as lizards, naked mole rats, and blind mole rats, possess stronger cardiovascular system-related oxygen transport capacity (He et al., 2013; Li et al., 2021a). Thus, combined with our findings on voles, we suggest that enhanced oxygen transport capacity may be a hypoxic adaptation strategy shared by species living in hypoxic environments. In terms of energy utilization, both the energy transformation strategy of *N. fuscus* (i.e., fatty acid oxidation to glucose oxidation) and oxygen-saving strategy of *L. brandtii* (i.e., reducing both fatty acid and glucose oxidation) under hypoxic environments have been confirmed laterally in other studies (Duan et al., 2021; Hochachka et al., 1996; Ivy et al., 2020; Schippers et al., 2012).

CONCLUSIONS

In the present study, we investigated the physiological and molecular responses of the cardiovascular system of two closely related rodents, *N. fuscus* and *L. brandtii*, under hypoxia (10% O_2 for 48 h) and normoxia (20.9% O_2 for 48 h), with *M. musculus* used for comparison. Results showed enhanced oxygen transport efficiency as a coping mechanism against hypoxia in *N. fuscus* and *L. brandtii*, but with some differences. Specifically, *N. fuscus* showed up-regulation of genes related to accelerated cardiac contraction and angiogenesis, whereas *L. brandtii* showed significant up-regulation of erythropoiesis-related genes. The synchronized up-regulation of hemoglobin synthesis-related genes was also observed in both species. We also found differences in cardiometabolic strategies against hypoxia. *Mus musculus* relied on ATP generation via fatty acid oxidation, whereas *N. fuscus* shifted energy production to glucose oxidation under hypoxic conditions and *L. brandtii* employed a conservative strategy involving down-regulation of fatty acid and glucose oxidation and a bradycardia phenotype. These strategies may help *N. fuscus* and *L. brandtii* conserve energy and cope with

hypoxia. Our findings suggest that the coping mechanisms of these closely related and hypoxia-tolerant species are context dependent.

DATA AVAILABILITY

The raw sequencing data were deposited in the NCBI under BioprojectID PRJNA787778 and in GSA under accession No. CRA006487 and in Science Data Bank under DOI: 10.11922 /sciencedb.01649.

SUPPLEMENTARY DATA

Supplementary data to this article can be found online.

COMPETING INTERESTS

The authors declare that they have no competing interests.

AUTHORS' CONTRIBUTIONS

L.Y.S. conceived and designed the study. X.J.L. and L.Y.S. analyzed the data, prepared the figures, and wrote the first manuscript draft. C.C.Q., B.J.C., and Z.L.W. participated in the revision of the manuscript. M.Y.L., P.C., M.L.H., C.X.C., Y.L., H.C., and M.W.J. were responsible for animal collection and husbandry. All authors read and approved the final version of the manuscript.

REFERENCES

Abdurrachim D, Luiken JJFP, Nicolay K, Glatz JFC, Prompers JJ, Nabben M. 2015. Good and bad consequences of altered fatty acid metabolism in heart failure: evidence from mouse models. *Cardiovascular Research*, **106**(2): 194−205.

Abu-Farha M, Niles J, Willmore WG. 2005. Erythroid-specific 5-aminolevulinate synthase protein is stabilized by low oxygen and proteasomal inhibition. *Biochemistry and Cell Biology*, **83**(5): 620−630.

Arakawa T, Kobayashi-Yurugi T, Alguel Y, Iwanari H, Hatae H, Iwata M, et al. 2015. Crystal structure of the anion exchanger domain of human erythrocyte band 3. *Science*, **350**(6261): 680−684.

Arieli R, Heth G, Nevo E, Zamir Y, Neutra O. 1986. Adaptive heart and breathing frequencies in 4 ecologically differentiating chromosomal species of mole rats in Israel. *Experientia*, **42**(2): 131−133.

Bai J, Liu CB, Zhu PJ, Li Y. 2021. Novel insights into molecular mechanism of mitochondria in diabetic cardiomyopathy. *Frontiers in Physiology*, **11**: 609157.

Barnett JM, McCollum GW, Penn JS. 2010. Role of cytosolic phospholipase A_2 in retinal neovascularization. *Investigative Ophthalmology & Visual Science*, **51**(2): 1136−1142.

Batista DS, Koehler AD, Romanel E, de Souza VC, Silva TD, Almeida MC, et al. 2019. De novo assembly and transcriptome of *Pfaffia glomerata* uncovers the role of photoautotrophy and the P450 family genes in 20-hydroxyecdysone production. *Protoplasma*, **256**(3): 601−614.

Bildyug N. 2019. Extracellular matrix in regulation of contractile system in cardiomyocytes. *International Journal of Molecular Sciences*, **20**(20): 5054.

Boosani CS, Sudhakar YA. 2011. Proteolytically derived endogenous angioinhibitors originating from the extracellular matrix. *Pharmaceuticals*, **4**(12): 1551−1577.

Brennan CM, Mazzucca NQ, Mezoian T, Hunt TM, Keane ML, Leonard JN, et al. 2014. Reduced heme levels underlie the exponential growth defect of the *Shewanella oneidensis hfq* mutant. *PLoS One*, **9**(10): e109879.

Brown N, Alkhayer K, Clements R, Singhal N, Gregory R, Azzam S, et al. 2016. Neuronal hemoglobin expression and its relevance to multiple sclerosis neuropathology. *Journal of Molecular Neuroscience*, **59**(1): 1−17.

Chen KY, Liu XJ, Bu PC, Lin CS, Rakhilin N, Locasale JW, et al. 2014. A metabolic signature of colon cancer initiating cells. *In*: Proceedings of 2014 36th Annual International Conference of the IEEE Engineering in Medicine and Biology Society. Chicago: IEEE, 4759–4762.

Chen MC, Chang JP, Lin YS, Pan KL, Ho WC, Liu WH, et al. 2016. Deciphering the gene expression profile of peroxisome proliferator-activated receptor signaling pathway in the left atria of patients with mitral regurgitation. *Journal of Translational Medicine*, **14**(1): 157.

Chen SF, Zhou YQ, Chen YR, Gu J. 2018. Fastp: an ultra-fast all-in-one FASTQ preprocessor. *Bioinformatics*, **34**(17): i884−i890.

Chen X, Zhang LB, Wang C. 2019. Prenatal hypoxia-induced epigenomic and transcriptomic reprogramming in rat fetal and adult offspring hearts. *Scientific Data*, **6**(1): 238.

Cheng Q, Huang CH, Cao H, Lin JL, Gong X, Li J, et al. 2019. A novel prognostic signature of transcription factors for the prediction in patients with GBM. *Frontiers in Genetics*, **10**: 906.

Conesa A, Götz S, García-Gómez JM, Terol J, Talón M, Robles M. 2005. Blast2GO: a universal tool for annotation, visualization and analysis in functional genomics research. *Bioinformatics*, **21**(18): 3674−3676.

Cox B, Tsamou M, Vrijens K, Neven KY, Winckelmans E, de Kok TM, et al. 2019. A Co-expression analysis of the placental transcriptome in association with maternal pre-pregnancy BMI and newborn birth weight. *Frontiers in Genetics*, **10**: 354.

Davidson NM, Oshlack A. 2014. Corset: enabling differential gene expression analysis for *de novo* assembled transcriptomes. *Genome Biology*, **15**(7): 410.

Diessler S, Jan M, Emmenegger Y, Guex N, Middleton B, Skene DJ, et al. 2018. A systems genetics resource and analysis of sleep regulation in the mouse. *PLoS Biology*, **16**(8): e2005750.

Dong QQ, Shi LY, Li YW, Jiang MW, Sun H, Wang BS, et al. 2018. Differential responses of *Lasiopodomys mandarinus* and *Lasiopodomys brandtii* to chronic hypoxia: a cross-species brain transcriptome analysis. *BMC Genomics*, **19**(1): 901.

Duan MQ, Wang ZM, Guo XY, Wang KJ, Liu SY, Zhang B, et al. 2021. Integrated analysis of transcriptomic and proteomic analyses reveals different metabolic patterns in the livers of Tibetan and Yorkshire pigs. *Animal Bioscience*, **34**(5): 922−930.

Fan TJ, Sun GH, Sun XD, Zhao LJ, Zhong RG, Peng YZ. 2019. Tumor energy metabolism and potential of 3-bromopyruvate as an inhibitor of aerobic glycolysis: implications in tumor treatment. *Cancers*, **11**(3): 317.

Frade AF, Teixeira PC, Ianni BM, Pissetti CW, Saba B, Wang LHT, et al. 2013. Polymorphism in the alpha cardiac muscle actin 1 gene is associated to susceptibility to chronic inflammatory cardiomyopathy. *PLoS One*, **8**(12): e83446.

Froese A, Breher SS, Waldeyer C, Schindler RFR, Nikolaev VO, Rinné S, et al. 2012. Popeye domain containing proteins are essential for stress-mediated modulation of cardiac pacemaking in mice. *The Journal of Clinical Investigation*, **122**(3): 1119−1130.

Grabherr MG, Haas BJ, Yassour M, Levin JZ, Thompson DA, Amit I, et al. 2011. Full-length transcriptome assembly from RNA-Seq data without a reference genome. *Nature Biotechnology*, **29**(7): 644−652.

Grimes KM, Voorhees A, Chiao YA, Han HC, Lindsey ML, Buffenstein R. 2014. Cardiac function of the naked mole-rat: ecophysiological responses to working underground. *American Journal of Physiology Heart and Circulatory Physiology*, **306**(5): H730−H737.

Grimes KM, Barefield DY, Kumar M, McNamara JW, Weintraub ST, de Tombe PP, et al. 2017. The naked mole-rat exhibits an unusual cardiac myofilament protein profile providing new insights into heart function of this naturally subterranean rodent. *Pflügers Archiv-European Journal of Physiology*, **469**(12): 1603−1613.

Haas BJ, Papanicolaou A, Yassour M, Grabherr M, Blood PD, Bowden J, et al. 2013. *De novo* transcript sequence reconstruction from RNA-seq using the Trinity platform for reference generation and analysis. *Nature Protocols*, **8**(8): 1494−1512.

He JZ, Xiu MH, Tang XL, Yue F, Wang NB, Yang SB, et al. 2013. The different mechanisms of hypoxic acclimatization and adaptation in Lizard *Phrynocephalus vlangalii* living on Qinghai-Tibet Plateau. *Journal of Experimental Zoology Part A:Ecological Genetics and Physiology*, **319**(3): 117−123.

He M, Cheng Y, Li W, Liu QS, Liu JX, Huang JH, et al. 2010. Vascular endothelial growth factor C promotes cervical cancer metastasis via up-regulation and activation of RhoA/ROCK-2/moesin cascade. *BMC Cancer*, **10**: 170.

Hermes-Lima M, Zenteno-Savín T. 2002. Animal response to drastic changes in oxygen availability and physiological oxidative stress. *Comparative Biochemistry and Physiology Part C:Toxicology & Pharmacology*, **133**(4): 537−556.

Hochachka PW, Clark CM, Holden JE, Stanley C, Ugurbil K, Menon RS. 1996. ^{31}P magnetic resonance spectroscopy of the Sherpa heart: a phosphocreatine/adenosine triphosphate signature of metabolic defense against hypobaric hypoxia. *Proceedings of the National Academy of Sciences of the United States of America*, **93**(3): 1215−1220.

Hofer T, Wenger RH, Kramer MF, Ferreira GC, Gassmann M. 2003. Hypoxic up-regulation of erythroid 5-aminolevulinate synthase. *Blood*, **101**(1): 348−350.

Hsiao YT, Shimizu I, Wakasugi T, Yoshida Y, Ikegami R, Hayashi Y, et al. 2021. Cardiac mitofusin-1 is reduced in non-responding patients with idiopathic dilated cardiomyopathy. *Scientific Reports*, **11**(1): 6722.

Huang H, Xie SW, Gu XL, Xiang B, Zhong ZF, Huang P, et al. 2021. Higher circulating miR-199a-5p indicates poor aerobic exercise capacity and associates with cardiovascular dysfunction during chronic exposure to high altitude. *Frontiers in Physiology*, **12**: 587241.

Huerta-Cepas J, Forslund K, Coelho LP, Szklarczyk D, Jensen LJ, von Mering C, et al. 2017. Fast genome-wide functional annotation through orthology assignment by eggNOG-Mapper. *Molecular Biology and Evolution*, **34**(8): 2115−2122.

Huerta-Cepas J, Szklarczyk D, Heller D, Hernández-Plaza A, Forslund SK, Cook H, et al. 2019. eggNOG 5.0: a hierarchical, functionally and phylogenetically annotated orthology resource based on 5090 organisms and 2502 viruses. *Nucleic Acids Research*, **47**(D1): D309−D314.

Iacobas DA, Fan CH, Iacobas S. 2008. Integrated transcriptomic response to cardiac chronic hypoxia: translation regulators and response to stress in cell survival. *Functional & Integrative Genomics*, **8**(3): 265−275.

Ilkovski B, Clement S, Sewry C, North KN, Cooper ST. 2005. Defining α-skeletal and α-cardiac actin expression in human heart and skeletal muscle explains the absence of cardiac involvement in *ACTA1* nemaline myopathy. *Neuromuscular Disorders*, **15**(12): 829−835.

Ivy CM, Sprenger RJ, Bennett NC, van Jaarsveld B, Hart DW, Kirby AM, et al. 2020. The hypoxia tolerance of eight related African mole-rat species rivals that of naked mole-rats, despite divergent ventilatory and metabolic strategies in severe hypoxia. *Acta Physiologica*, **228**(4): e13436.

Jeckel KM, Bouma GJ, Hess AM, Petrilli EB, Frye MA. 2014. Dietary fatty acids alter left ventricular myocardial gene expression in Wistar rats. *Nutrition Research*, **34**(8): 694−706.

Kashyap M, Yoshimura N, Smith PP, Chancellor M, Tyagi P. 2015. Characterization of the role of HCN channels in β3-adrenoceptor mediated rat bladder relaxation. *Bladder*, **2**(2): e15.

Katano W, Moriyama Y, Takeuchi JK, Koshiba-Takeuchi K. 2019. Cardiac septation in heart development and evolution. *Development, Growth & Differentiation*, **61**(1): 114−123.

Khechaduri A, Bayeva M, Chang HC, Ardehali H. 2013. Heme levels are increased in human failing hearts. *Journal of the American College of Cardiology*, **61**(18): 1884−1893.

Khodaee M, Grothe HL, Seyfert JH, VanBaak K. 2016. Athletes at high altitude. *Sports Health:A Multidisciplinary Approach*, **8**(2): 126−132.

Kirby AM, Fairman GD, Pamenter ME. 2018. Atypical behavioural, metabolic and thermoregulatory responses to hypoxia in the naked mole rat (*Heterocephalus glaber*). *Journal of Zoology*, **305**(2): 106−115.

Koga T, Sasaki F, Saeki K, Tsuchiya S, Okuno T, Ohba M, et al. 2021. Expression of leukotriene B_4 receptor 1 defines functionally distinct DCs that control allergic skin inflammation. *Cellular & Molecular Immunology*, **18**(6): 1437−1449.

Kolwicz SC Jr, Olson DP, Marney LC, Garcia-Menendez L, Synovec RE, Tian R. 2012. Cardiac-specific deletion of acetyl CoA carboxylase 2 prevents metabolic remodeling during pressure-overload hypertrophy. *Circulation Research*, **111**(6): 728−738.

Kong XY, Dong XX, Yang SL, Qian JH, Yang JF, Jiang Q, et al. 2019. Natural selection on TMPRSS6 associated with the blunted erythropoiesis and improved blood viscosity in Tibetan pigs. *Comparative Biochemistry and Physiology Part B:Biochemistry and Molecular Biology*, **233**: 11−22.

Kryczek I, Lange A, Mottram P, Alvarez X, Cheng P, Hogan M, et al. 2005. CXCL12 and vascular endothelial growth factor synergistically induce neoangiogenesis in human ovarian cancers. *Cancer Research*, **65**(2): 465−472.

Kurniawan H, Soriano-Baguet L, Brenner D. 2020. Regulatory T cell metabolism at the intersection between autoimmune diseases and cancer. *European Journal of Immunology*, **50**(11): 1626−1642.

Lau GY, Arndt S, Murphy MP, Richards JG. 2019. Species- and tissue-specific differences in ROS metabolism during exposure to hypoxia and hyperoxia plus recovery in marine sculpins. *Journal of Experimental Biology*, **222**(Pt 22): jeb206896.

Lavergne A, Tarifeño-Saldivia E, Pirson J, Reuter AS, Flasse L, Manfroid I, et al. 2020. Pancreatic and intestinal endocrine cells in zebrafish share common transcriptomic signatures and regulatory programmes. *BMC Biology*, **18**(1): 109.

Lawler J. 2002. Thrombospondin-1 as an endogenous inhibitor of angiogenesis and tumor growth. *Journal of Cellular and Molecular Medicine*, **6**(1): 1−12.

Li B, Dewey CN. 2011. RSEM: accurate transcript quantification from RNA-Seq data with or without a reference genome. *BMC Bioinformatics*, **12**(1): 323.

Li F, Xu RJ, Low BE, Lin CL, Garcia-Barros M, Schrandt J, et al. 2018. Alkaline ceramidase 2 is essential for the homeostasis of plasma sphingoid bases and their phosphates. *The FASEB Journal*, **32**(6): 3058−3069.

Li MK, Pan D, Sun H, Zhang L, Cheng H, Shao T, et al. 2021a. The hypoxia adaptation of small mammals to plateau and underground burrow conditions. *Animal Models and Experimental Medicine*, **4**(4): 319−328.

Li MY, Tian XY, Li XJ, Huang ML, Huang S, Wu Y, et al. 2021b. Diverse energy metabolism patterns in females in *Neodon fuscus, Lasiopodomys brandtii*, and *Mus musculus* revealed by comparative transcriptomics under hypoxic conditions. *Science of the Total Environment*, **783**: 147130.

Li W, Dong YN, Dong QQ, Sun H, Zhang YF, Wang ZL. 2021c. The remarkable hypoxia tolerance in Brandt's voles (*Lasiopodomys brandtii*).

European Journal of Neuroscience, **53**(5): 1652−1660.
Liu B, Wang ZL, Lu JQ. 2010. Response to chronic intermittent hypoxia in blood system of Mandarin vole (*Lasiopodomys mandarinus*). *Comparative Biochemistry and Physiology Part A:Molecular & Integrative Physiology*, **156**(4): 469−474.
Liu CC, Niu YL, Zhou XD, Xu X, Yang Y, Zhang Y, et al. 2015. Cell cycle control, DNA damage repair, and apoptosis-related pathways control pre-ameloblasts differentiation during tooth development. *BMC Genomics*, **16**(1): 592.
Liu J, Huang SL, Li GL, Zhao JD, Lu W, Zhang ZB. 2020. High housing density increases stress hormone- or disease-associated fecal microbiota in male Brandt's voles (*Lasiopodomys brandtii*). *Hormones and Behavior*, **126**: 104838.
Long Y, Yan JJ, Song GL, Li XH, Li XX, Li Q, et al. 2015. Transcriptional events co-regulated by hypoxia and cold stresses in Zebrafish larvae. *BMC Genomics*, **16**(1): 385.
López-Barneo J, Pardal R, Ortega-Sáenz P. 2001. Cellular mechanism of oxygen sensing. *Annual Review of Physiology*, **63**: 259−287.
Lorenzo O, Ramírez E, Picatoste B, Egido J, Tuñón J. 2013. Alteration of energy substrates and ROS production in diabetic cardiomyopathy. *Mediators of Inflammation*, **2013**: 461967.
Love MI, Huber W, Anders S. 2014. Moderated estimation of fold change and dispersion for RNA-seq data with DESeq2. *Genome Biology*, **15**(12): 550.
Ludwig LS, Khajuria RK, Sankaran VG. 2016. Emerging cellular and gene therapies for congenital anemias. *American Journal of Medical Genetics Part C:Seminars in Medical Genetics*, **172**(4): 332−348.
Lv L, Deng H, Li Y, Zhang C, Liu X, Liu Q, et al. 2014. The DNA methylation-regulated miR-193a-3p dictates the multi-chemoresistance of bladder cancer via repression of SRSF2/PLAU/HIC2 expression. *Cell Death & Disease*, **5**(9): e1402.
Ma H, Yu S, Liu XJ, Zhang YG, Fakadej T, Liu ZQ, et al. 2019. Lin28a regulates pathological cardiac hypertrophic growth through Pck2-mediated enhancement of anabolic synthesis. *Circulation*, **139**(14): 1725−1740.
Majmundar AJ, Wong WJ, Simon MC. 2010. Hypoxia-inducible factors and the response to hypoxic stress. *Molecular Cell*, **40**(2): 294−309.
Martínez-Micaelo N, González-Abuín N, Terra X, Ardévol A, Pinent M, Petretto E, et al. 2016. Identification of a nutrient-sensing transcriptional network in monocytes by using inbred rat models on a cafeteria diet. *Disease Models & Mechanisms*, **9**(10): 1231−1239.
Mehta V, Fields L, Evans IM, Yamaji M, Pellet-Many C, Jones T, et al. 2018. VEGF (vascular endothelial growth factor) induces NRP1 (neuropilin-1) cleavage via ADAMs (a disintegrin and metalloproteinase) 9 and 10 to generate novel carboxy-terminal NRP1 fragments that regulate angiogenic signaling. *Arteriosclerosis, Thrombosis, and Vascular Biology*, **38**(8): 1845−1858.
Milanesi R, Bucchi A, Baruscotti M. 2015. The genetic basis for inherited forms of sinoatrial dysfunction and atrioventricular node dysfunction. *Journal of Interventional Cardiac Electrophysiology*, **43**(2): 121−134.
Miller D, Hannon C, Ganetzky B. 2012. A mutation in *Drosophila* aldolase causes temperature-sensitive paralysis, shortened lifespan, and neurodegeneration. *Journal of Neurogenetics*, **26**(3-4): 317−327.
Miyata S, Minobe W, Bristow MR, Leinwand LA. 2000. Myosin heavy chain isoform expression in the failing and nonfailing human heart. *Circulation Research*, **86**(4): 386−390.
Moriya Y, Itoh M, Okuda S, Yoshizawa AC, Kanehisa M. 2007. KAAS: an automatic genome annotation and pathway reconstruction server. *Nucleic Acids Research*, **35**(S2): W182−W185.
Orso F, Balzac F, Marino M, Lembo A, Retta SF, Taverna D. 2013. miR-21 coordinates tumor growth and modulates KRIT1 levels. *Biochemical and Biophysical Research Communications*, **438**(1): 90−96.
Pamenter ME, Lau GY, Richards JG, Milsom WK. 2018. Naked mole rat brain mitochondria electron transport system flux and H^+ leak are reduced during acute hypoxia. *Journal of Experimental Biology*, **221**(4): jeb171397.
Pamidimukkala NV, Leonard MK, Snyder D, McCorkle JR, Kaetzel DM. 2018. Metastasis suppressor NME1 directly activates transcription of the *ALDOC* gene in melanoma cells. *Anticancer Research*, **38**(11): 6059−6068.
Paparde A, Plakane L, Circenis K, Aivars JI. 2015. Effect of acute systemic hypoxia on human cutaneous microcirculation and endothelial, sympathetic and myogenic activity. *Microvascular Research*, **102**: 1−5.
Paul DS, Grevengoed TJ, Pascual F, Ellis JM, Willis MS, Coleman RA. 2014. Deficiency of cardiac Acyl-CoA synthetase-1 induces diastolic dysfunction, but pathologic hypertrophy is reversed by rapamycin. *Biochimica et Biophysica Acta* (*BBA*) - *Molecular and Cell Biology of Lipids*, **1841**(6): 880–887.
Pell VR, Chouchani ET, Murphy MP, Brookes PS, Krieg T. 2016. Moving forwards by blocking back-flow: the Yin and Yang of MI therapy. *Circulation Research*, **118**(5): 898−906.
Peoples JN, Saraf A, Ghazal N, Pham TT, Kwong JQ. 2019. Mitochondrial dysfunction and oxidative stress in heart disease. *Experimental & Molecular Medicine*, **51**(12): 1−13.
Pichon A, Bai ZZ, Marchant D, Jin GE, Voituron N, Yu HX, et al. 2013. Cardiac adaptation to high altitude in the plateau pika (*Ochotona curzoniae*). *Physiological Reports*, **1**(2): e00032.
Potter JHT, Davies KTJ, Yohe LR, Sanchez MKR, Rengifo EM, Struebig M, et al. 2021. Dietary diversification and specialization in neotropical bats facilitated by early molecular evolution. *Molecular Biology and Evolution*, **38**(9): 3864−3883.
Qu YL, Deng CH, Luo Q, Shang XY, Wu JX, Shi Y, et al. 2019. *Arid1a* regulates insulin sensitivity and lipid metabolism. *eBioMedicine*, **42**: 481−493.
Roklicer R, Lakicevic N, Stajer V, Trivic T, Bianco A, Mani D, et al. 2020. The effects of rapid weight loss on skeletal muscle in judo athletes. *Journal of Translational Medicine*, **18**(1): 142.
Sawada N, Li YX, Liao JK. 2010. Novel aspects of the roles of Rac1 GTPase in the cardiovascular system. *Current Opinion in Pharmacology*, **10**(2): 116−121.
Schindler RFR, Brand T. 2016. The Popeye domain containing protein family-A novel class of cAMP effectors with important functions in multiple tissues. *Progress in Biophysics and Molecular Biology*, **120**(1-3): 28−36.
Schippers MP, Ramirez O, Arana M, Pinedo-Bernal P, McClelland GB. 2012. Increase in carbohydrate utilization in high-altitude Andean mice. *Current Biology*, **22**(24): 2350−2354.
Schneider AM, Duffield AS, Symer DE, Burns KH. 2009. Roles of retrotransposons in benign and malignant hematologic disease. *Cellscience*, **6**(2): 121−145.
Scott GR, Hawkes LA, Frappell PB, Butler PJ, Bishop CM, Milsom WK. 2015. How bar-headed geese fly over the Himalayas. *Physiology*, **30**(2): 107−115.
Shannon P, Markiel A, Ozier O, Baliga NS, Wang JT, Ramage D, et al. 2003. Cytoscape: a software environment for integrated models of biomolecular interaction networks. *Genome Research*, **13**(11): 2498−2504.
Shao X, Dong X, Cai J, Tang C, Xie KN, Yan ZD, et al. 2021. Oxygen enrichment ameliorates cardiorespiratory alterations induced by chronic high-altitude hypoxia in rats. *Frontiers in Physiology*, **11**: 616145.
Shi LY, Liu LK, Li XJ, Wu Y, Tian XY, Shi YH, et al. 2021a. Phylogeny and evolution of *Lasiopodomys* in subfamily Arvivolinae based on mitochondrial genomics. *PeerJ*, **9**: e10850.

Shi LY, Jiang MW, Li MY, Shang XZ, Li XJ, Huang ML, et al. 2021b. Regulation of HIF-1α and p53 in stress responses in the subterranean rodents *Lasiopodomys mandarinus* and *Lasiopodomys brandtii* (Rodentia: Cricetidae). *Zoologia*, **38**: e58607.

Shi LY, Chen BJ, Wang XR, Huang ML, Qiao CC, Wang JG, et al. 2021c. Antioxidant response to severe hypoxia in Brandt's vole *Lasiopodomys brandtii*. *Integrative Zoology*, **00**: 1–15.

Shinzawa-Itoh K, Shimomura rt H, Yanagisawa S, Shimada S, Takahashi R, Oosaki M, et al. 2016. Purification of active respiratory supercomplex from bovine heamitochondria enables functional studies. *Journal of Biological Chemistry*, **291**(8): 4178−4184.

Simão FA, Waterhouse RM, Ioannidis P, Kriventseva EV, Zdobnov EM. 2015. BUSCO: assessing genome assembly and annotation completeness with single-copy orthologs. *Bioinformatics*, **31**(19): 3210−3212.

Sindi HA, Russomanno G, Satta S, Abdul-Salam VB, Jo KB, Qazi-Chaudhry B, et al. 2020. Therapeutic potential of KLF2-induced exosomal microRNAs in pulmonary hypertension. *Nature Communications*, **11**(1): 1185.

Singh NK, Rao GN. 2019. Emerging role of 12/15-Lipoxygenase (ALOX15) in human pathologies. *Progress in Lipid Research*, **73**: 28−45.

Su ZH, Liu YW, Zhang H. 2021. Adaptive cardiac metabolism under chronic hypoxia: mechanism and clinical implications. *Frontiers in Cell and Developmental Biology*, **9**: 625524.

Sun KQ, Zhang YJ, D'Alessandro A, Nemkov T, Song AR, Wu HY, et al. 2016. Sphingosine-1-phosphate promotes erythrocyte glycolysis and oxygen release for adaptation to high-altitude hypoxia. *Nature Communications*, **7**(1): 12086.

Sun W, Liu CX, Chen QH, Liu N, Yan YY, Liu B. 2018. SIRT3: a new regulator of cardiovascular diseases. *Oxidative Medicine and Cellular Longevity*, **2018**: 7293861.

Suzuki TA, Martins FM, Nachman MW. 2019. Altitudinal variation of the gut microbiota in wild house mice. *Molecular Ecology*, **28**(9): 2378−2390.

Thompson CB. 2016. Into thin air: how we sense and respond to hypoxia. *Cell*, **167**(1): 9−11.

Toyono T, Usui T, Yokoo S, Taketani Y, Nakagawa S, Kuroda M, et al. 2015. Angiopoietin-like 7 is an anti-angiogenic protein required to prevent vascularization of the cornea. *PLoS One*, **10**(1): e0116838.

Trindade A, Duarte A. 2020. Notch signaling function in the angiocrine regulation of tumor development. *Cells*, **9**(11): 2467.

Verghese J. 2013. Slaying dementia dragons with blood, lungs, and guts. *Journal of the American Geriatrics Society*, **61**(1): 155−157.

Wang H, Zhong JC, Wang JK, Chai ZX, Zhang CF, Xin JW, et al. 2021. Whole-transcriptome analysis of yak and cattle heart tissues reveals regulatory pathways associated with high-altitude adaptation. *Frontiers in Genetics*, **12**: 579800.

Wang L, Song LJ, Li C, Feng QL, Xu MP, Li ZQ, et al. 2018. Renal denervation improves cardiac function by attenuating myocardiocyte apoptosis in dogs after myocardial infarction. *BMC Cardiovascular Disorders*, **18**(1): 86.

Wang SF, Yu XP, Lin ZH, Zhang SQ, Xue LY, Xue QG, et al. 2017a. Hemoglobins likely function as peroxidase in blood clam *Tegillarca granosa* hemocytes. *Journal of Immunology Research*, **2017**: 7125084.

Wang ZX, Shang P, Li QG, Wang LY, Chamba Y, Zhang B, et al. 2017b. iTRAQ-based proteomic analysis reveals key proteins affecting muscle growth and lipid deposition in pigs. *Scientific Reports*, **7**: 46717.

Wu Z, Jin FY, Wang LX, Zhao YF, Jiang Y, Li J, et al. 2019. Antioxidant effects of *baoyuan* decoction on dysfunctional erythrocytes in high-fat diet-induced hyperlipidemic ApoE$^{-/-}$ Mice. *Oxidative Medicine and Cellular Longevity*, **2019**: 5172480.

Xu LL, Hao ZQ, Lin JY, Zhao Q, Zhang BJ, Li GL, et al. 2019. Transcriptome sequencing of *Eospalax fontanierii* to determine hypoxia regulation of cardiac fibrinogen. *Molecular Biology Reports*, **46**(6): 5671−5683.

Xu-Cai YO, Wu QY. 2010. Molecular forms of natriuretic peptides in heart failure and their implications. *Heart*, **96**(6): 419−424.

Yan W, Wu FY, Morser J, Wu QY. 2000. Corin, a transmembrane cardiac serine protease, acts as a pro-atrial natriuretic peptide-converting enzyme. *Proceedings of the National Academy of Sciences of the United States of America*, **97**(15): 8525−8529.

Yang X, Zhang H, Shang J, Liu G, Xia T, Zhao C, et al. 2018. Comparative analysis of the blood transcriptomes between wolves and dogs. *Animal Genetics*, **49**(4): 291−302.

Yčas JW, Horrow JC, Horne BD. 2015. Persistent increase in red cell size distribution width after acute diseases: a biomarker of hypoxemia. *Clinica Chimica Acta*, **448**: 107−117.

Yin ZY, Ren J, Guo W. 2015. Sarcomeric protein isoform transitions in cardiac muscle: a journey to heart failure. *Biochimica et Biophysica Acta* (*BBA*) - *Molecular Basis of Disease*, **1852**(1): 47–52.

Yoon HE, Kim SJ, Hwang HS, Chung S, Yang CW, Shin SJ. 2015. Progressive rise in red blood cell distribution width predicts mortality and cardiovascular events in end-stage renal disease patients. *PLoS One*, **10**(5): e0126272.

Zeng CJ, Li WJ, Liao Q, Yan TT, Wang KS, Hu Y, et al. 2019. Comparative transcriptomics reveals the expression differences between four developmental stages of American cockroach (*Periplaneta americana*). *DNA and Cell Biology*, **38**(10): 1078−1087.

Zhang J, Malmirchegini GR, Clubb RT, Loo JA. 2015. Native top-down mass spectrometry for the structural characterization of human hemoglobin. *European Journal of Mass Spectrometry*, **21**(3): 221−231.

Zhang XX, Lou ZZ, Huang SY, Zhou DH, Jia WZ, Su CL, et al. 2013. Genetic characterization of *Toxoplasma gondii* from Qinghai vole, Plateau pika and Tibetan ground-tit on the Qinghai-Tibet Plateau, China. *Parasites & Vectors*, **6**: 291.

Zhang XY, Jian YN, Li XP, Ma LQ, Karanis G, Karanis P. 2018. The first report of *Cryptosporidium* spp. in *Microtus fuscus* (Qinghai vole) and *Ochotona curzoniae* (wild plateau pika) in the Qinghai-Tibetan Plateau area, China. *Parasitology Research*, **117**(5): 1401−1407.

Zhang Y, Zhang HL, Zhang B, Ling Y, Zhang H. 2020. Identification of key HIF-1α target genes that regulate adaptation to hypoxic conditions in Tibetan chicken embryos. *Gene*, **729**: 144321.

Zheng XG, Chopp M, Lu Y, Buller B, Jiang F. 2013. MiR-15b and miR-152 reduce glioma cell invasion and angiogenesis via NRP-2 and MMP-3. *Cancer Letters*, **329**(2): 146−154.